
Electrocatalytic Oxygen Reduction Reaction

Chaojie Song and Jiujuan Zhang

2.1 Introduction

Oxygen (O_2) is the most abundant element in the Earth's crust. The oxygen reduction reaction (ORR) is also the most important reaction in life processes such as biological respiration, and in energy converting systems such as fuel cells. ORR in aqueous solutions occurs mainly by two pathways: the direct 4-electron reduction pathway from O_2 to H_2O , and the 2-electron reduction pathway from O_2 to hydrogen peroxide (H_2O_2). In non-aqueous aprotic solvents and/or in alkaline solutions, the 1-electron reduction pathway from O_2 to superoxide ($O_2^{\cdot-}$) can also occur.

In proton exchange membrane (PEM) fuel cells, including direct methanol fuel cells (DMFCs), ORR is the reaction occurring at the cathode. Normally, the ORR kinetics is very slow. In order to speed up the ORR kinetics to reach a practical usable level in a fuel cell, a cathode ORR catalyst is needed. At the current stage in technology, platinum (Pt)-based materials are the most practical catalysts. Because these Pt-based catalysts are too expensive for making commercially viable fuel cells, extensive research over the past several decades has focused on developing alternative catalysts, including non-noble metal catalysts [1]. These electrocatalysts include noble metals and alloys, carbon materials, quinone and derivatives, transition metal macrocyclic compounds, transition metal chalcogenides, and transition metal carbides. In this chapter, we focus on the O_2 reduction reaction, including the reaction kinetics and mechanisms catalyzed by these various catalysts.

To assist readers, we first provide an overview of the following background information: the major electrochemical O_2 reduction reaction processes, simple ORR kinetics, and conventional techniques for electrochemical measurements.

2.1.1 Electrochemical O_2 Reduction Reactions [2, 3]

Table 2.1 lists several typical ORR processes with their corresponding thermodynamic electrode potentials at standard conditions. The mechanism of the electrochemical O_2 reduction reaction is quite complicated and involves many

intermediates, primarily depending on the natures of the electrode material, catalyst, and electrolyte. The mechanism catalyzed by different catalysts is discussed in detail later in this chapter.

Table 2.1. Thermodynamic electrode potentials of electrochemical O₂ reductions [2, 3]

Electrolyte	ORR reactions	Thermodynamic electrode potential at standard conditions, V
Acidic aqueous solution	$O_2 + 4H^+ + 4e^- \rightarrow H_2O$	1.229
	$O_2 + 2H^+ + 2e^- \rightarrow H_2O_2$	0.70
	$H_2O_2 + 2H^+ + 2e^- \rightarrow 2H_2O$	1.76
Alkaline aqueous solution	$O_2 + H_2O + 4e^- \rightarrow 4OH^-$	0.401
	$O_2 + H_2O + 2e^- \rightarrow HO_2^- + OH^-$	-0.065
	$HO_2^- + H_2O + 2e^- \rightarrow 3OH^-$	0.867
Non-aqueous aprotic solvents	$O_2 + e^- \rightarrow O_2^-$	a
	$O_2^- + e^- \rightarrow O_2^{2-}$	b

a, b: The thermodynamic potentials for the 1-electron reduction reaction to form a superoxide, and its further reduction to O₂²⁻, are not listed in Table 2.1 because their values are strongly dependent on the solvent used.

In Table 2.1, the reduction pathways such as the 1-, 2-, and 4-electron reduction pathways have unique significance, depending on the applications. In fuel cell processes, the 4-electron direct pathway is highly preferred. The 2-electron reduction pathway is used in industry for H₂O₂ production. The 1-electron reduction pathway is of importance in the exploration of the ORR mechanism.

2.1.2 Kinetics of the O₂ Reduction Reaction

It is desirable to have the O₂ reduction reaction occurring at potentials as close as possible to the reversible electrode potential (thermodynamic electrode potential) with a satisfactory reaction rate. The current-overpotential is given in Equation 2.1 [3]:

$$I_c = i_{O_2}^o \left(e^{\frac{n_{\alpha O} \alpha_o F \eta_c}{RT}} - e^{-\frac{n_{\alpha O} (1 - \alpha_o) F \eta_c}{RT}} \right) \quad (2.1)$$

where I_c is the oxygen reduction reaction current density, $i_{O_2}^o$ is the exchange current density, $n_{\alpha O}$ is the number of electrons transferred in the rate determining step, α_o is the transfer coefficient, η_c is the overpotential of ORR, F is the Faraday constant, R is the gas constant, and T is the temperature in Kelvin. To obtain high

current at low overpotential, the exchange current density $i_{O_2}^0$ should be large, and/or $\frac{RT}{\alpha_o n_{ao} F}$ should be small.

2.1.2.1 Tafel Slope

If the overpotential is large, the backward reaction is negligible and Equation 2.1 can be simplified as

$$I_c = i_{O_2}^0 e^{\frac{n_{ao} \alpha_o F \eta_c}{RT}} \quad (2.2)$$

The plot of $\eta_c \sim \log(I_c)$ gives a linear relationship, and the slope is $\frac{2.303RT}{\alpha_o n_{ao} F}$.

This slope is called the Tafel slope. Since all other parameters in the Tafel slope are known, the parameters determining the Tafel slope are actually α_o and n_{ao} . The higher the Tafel slope, the faster the overpotential increases with the current density. Thus, for an electrochemical reaction to obtain a high current at low overpotential, the reaction should exhibit a low Tafel slope or a large $\alpha_o n_{ao}$. For ORR, usually two Tafel slopes are obtained, 60 mV/dec and 120 mV/dec, respectively, depending on the electrode materials used and on the potential range. Details for individual materials are given in later sections of this chapter. The electron transfer coefficient is a key factor determining the Tafel slope. For ORR, the transfer coefficient is dependent on temperature. On a Pt electrode, the transfer coefficient of ORR increases linearly with temperature in the range of 20–250 °C, following Equation 2.3 [4, 5]:

$$\alpha_o = \alpha_o^0 T \quad (2.3)$$

where α_o is the electron transfer coefficient of ORR, α_o^0 equals 0.001678, and T is temperature in Kelvin. Relative humidity (RH) has also been found to affect the transfer coefficient [6]. Our recent study showed that in PEMFCs, at 120 °C the RH dependence of transfer coefficient change for ORR follows Equation 2.4:

$$\alpha_o = (0.001552 RH_c + 0.000139) T \quad (2.4)$$

where RH_c is the relative humidity of the cathode compartment.

2.1.2.2 Exchange Current Density

Exchange current density is an important kinetic parameter representing the electrochemical reaction rate at equilibrium. For an electrochemical reaction,



both forward and backward reactions can occur. At equilibrium, the net current density of the reaction is zero. The current density of the forward reaction equals that of the backward reaction [3]. This current density is called exchange current density. The magnitude of the exchange current density determines how rapidly the electrochemical reaction can occur.

The exchange current density of an electrochemical reaction depends on the reaction and on the electrode surface on which the electrochemical reaction occurs. For example, on a Pt electrode, the exchange current density of hydrogen oxidation is several orders larger than that of ORR. The O_2 reduction reaction shows a higher exchange current density on a Pt electrode than on an Au electrode. Therefore, electrode materials or catalysts have a strong effect on ORR kinetics. Different materials can give different exchange current densities. Table 2.2 lists the ORR exchange current densities on various electrode materials.

Table 2.2. ORR exchange current densities on various electrode materials

Electrode material /catalyst	ORR exchange current density, $A.cm^{-2}$	Electron transfer co-efficiency	Electron transfer num. in rate determining step	Measurement conditions	Ref.
Pt	2.8×10^{-7}	0.48	-	At Pt/Nafion interface at 30 °C	7
PtO/Pt	1.7×10^{-10}	0.46	-	At Pt/Nafion interface at 30 °C	7
FePc	1.3×10^{-7}	-	-	In pH 1.3 solution	61
PtFe/C	2.15×10^{-7}	0.55	1	In 0.5 M H_2SO_4 at 60 °C	47
PtW ₂ C/C	4.7×10^{-7}	0.45	2	In 0.5 M H_2SO_4 at 25 °C	75
	5.0×10^{-5}	0.47	1		
Ru _x Se _y	2.22×10^{-8}	0.52	1	In 0.5 M H_2SO_4 at 25 °C	67
Ru _x Fe _y Se _z	4.47×10^{-8}	0.51	1	In 0.5 M H_2SO_4 at 25 °C	68

The exchange current density is related to the true electrode area and to the reactant concentration (or partial pressure, for a gas), especially for ORR on the Pt electrode in fuel cells. The true electroactive area of Pt is significantly different from its geometric area, and the partial pressure of O_2 is not 1 atm. Thus, the intrinsic exchange current density should be used, which is shown in Equation 2.6 [4]:

$$i_{O_2}^{o-\text{apparent}} = (EP\text{SA})_c i_{O_2}^o \left(\frac{P_{O_2}}{P_{O_2}^o} \right)^{\alpha_o} \quad (2.6)$$

where $i_{O_2}^{o-\text{apparent}}$ is the apparent exchange current density; $(EP\text{SA})_c$ is the electroactive Pt surface area of the cathode catalyst; $i_{O_2}^o$ is the intrinsic exchange current density; $P_{O_2}^o$ is the standard O_2 partial pressure; P_{O_2} is the actual O_2 pressure; and α_o is the transfer coefficient of ORR. Since the apparent exchange current density does not reflect the true situation of ORR, hereafter all reference to exchange current density will be to the intrinsic exchange current density.

The exchange current density is also temperature dependent. The relationship between exchange current density and temperature follows the Arrhenius equation,

$$i_{O_2}^o = I_{O_2}^0 e^{-(E_a/RT)} \quad (2.7)$$

where $I_{O_2}^0$ is the exchange current density at $T = \infty$, E_a is the activation energy, and R , T have their usual significance. Studies on the temperature dependence of ORR on Pt electrodes have been investigated both in half-cells and in fuel cells. Parthasarathy et al. [7] investigated the temperature dependence of ORR kinetics at the Pt/Nafion interface, and Wakabayashi et al. [8] studied the temperature dependence of ORR kinetics at a Pt electrode in an acidic solution. Recently, we studied ORR kinetics in a wide temperature range (from 23 °C–120 °C) in PEMFCs [4]. A wide range of ORR activation energy has been reported: from 21 to 83 kJ/mol for both Tafel regions, depending on the catalyst and method used. We reported values of 28.3 kJ/mol on a PtO/Pt surface and of 57.3 kJ/mol on a pure Pt surface, measured in a fuel cell environment [4].

2.1.3 Techniques Used in Electrocatalytic O_2 Reduction Reactions

The most frequently used techniques for ORR catalysis studies are steady-state polarization, cyclic voltammetry, rotating disk electrode (RDE), and rotating ring-disk electrode (RRDE).

2.1.3.1 Steady-state Polarization

Polarization means that the potential of the electrode surface shifts away from its equilibrium value, leading to an electrochemical reaction. In general, for an elementary electrochemical reaction, $O + e^- \leftrightarrow R$, the polarization follows the Butler-Volmer equation [3]:

$$i = i^0 \left(e^{\frac{\beta F \eta_c}{RT}} - e^{-\frac{(1-\beta) F \eta_c}{RT}} \right) \quad (2.8)$$

where i^0 is the exchange current density, η_c is the overpotential for the reduction of reactant O, and β is the symmetry factor. In the reaction, only part of the overpotential activates the forward reaction, and the symmetry factor represents the fraction of the overpotential affecting the forward reaction. All other parameters have their usual significance.

Most of the electrochemical reactions, however, are not elementary, especially for multiple electron transfer reactions. Even a 1-electron transfer reaction may involve several other steps. The whole reaction consists of multiple elementary reactions, including electron transfer steps and chemical steps. Each elementary reaction has a reaction rate. Each elementary step involving electron transfer gives a Butler-Volmer equation, and each chemical step gives a reaction rate equation. The whole reaction rate or electrochemical current is determined by the slowest step. Other steps also contribute to the whole reaction rate, depending on their reaction rates. Deduction of the whole reaction rate is complicated. In some cases, a chemical step is the rate determining step (rds). For example, in a carbon catalyzed ORR, adsorbed superoxide migration might be the rds (see Section 2.2, below). To simplify, for an electrochemical reaction involving multiple electron transfer, the rate determining step is considered a pseudo-elementary step with an electron transfer number of n . For ORR, n might be 1 or 2, depending on the catalysts used and the potential range. This pseudo-elementary step gives a current-overpotential relationship, as shown in Equation 2.9:

$$i = i^0 \left(e^{\frac{\alpha n F \eta_c}{RT}} - e^{-\frac{(1-\alpha) n F \eta_c}{RT}} \right) \quad (2.9)$$

where n is the electron transfer number in the pseudo-elementary rate determining step, and α is the transfer coefficient representing the fraction of overpotential that activates the forward direction of the pseudo-elementary rate determining step. The exchange current density and Tafel slope have already been explained in Section 2.1.2.

A steady-state polarization curve describes the relationship between the electrode potential and the current density, which is recorded by either holding the electrode potential and recording the stable current response, or holding the current density and recording the stable potential response. The criteria to evaluate a polarization curve depend on its application. In fuel cells, for both ORR and fuel cell performance, high current density is expected at lower overpotential (ORR) or at higher cell voltage (fuel cell), which gives maximum power density. Figure 2.1 shows the steady-state polarization curves of a PEMFC at 23 °C and 80 °C [4]. At any current density, cell voltage obtained at 80 °C is higher than that at 23 °C, indicating the fuel cell shows better performance at 80 °C than at 23 °C. Fitting the polarization curves or plotting the overpotential vs. $\log(I)$ gives the Tafel slope and the exchange current density. We fitted the polarization curves of PEMFCs at low current density range ($< 0.4 \text{ A/cm}^2$) and at high current density range ($> 0.4 \text{ A/cm}^2$), which resulted in two exchange current densities. For example, at 80 °C, on a PtO/Pt surface ($< 0.4 \text{ A/cm}^2$), an exchange current density of $6.25 \times 10^{-6} \text{ A/cm}^2$

was obtained for ORR, and on a Pt surface ($> 0.4 \text{ A/cm}^2$), an exchange current density of $5.26 \times 10^{-6} \text{ A/cm}^2$ was obtained [4].

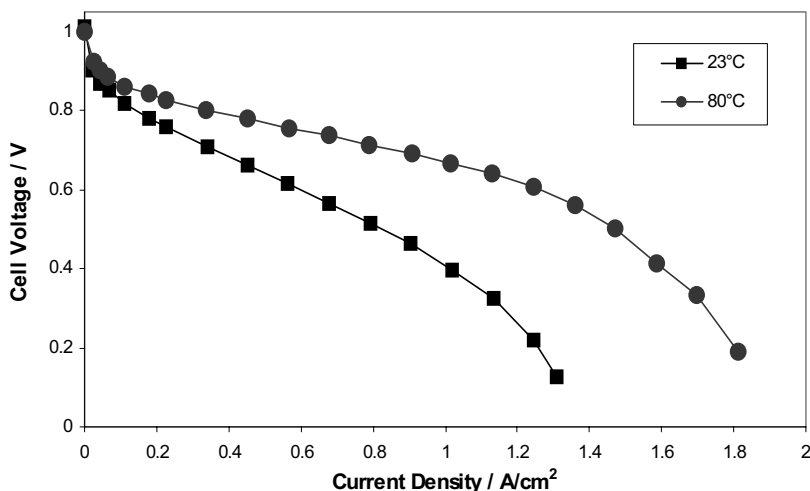


Figure 2.1. Polarization curves obtained at 23 °C and 80 °C with a backpressure of 30 psig. MEA active area: 4.4 cm^2 . H_2/Air gases with 100% relative humidity, adapted from [4]. (Reprinted from *Electrochimica Acta*, 52(7), Song C, Tang Y, Zhang J, Zhang J, Wang H, Shen J, et al., PEM fuel cell reaction kinetics in the temperature range of 23–120 °C, 2552–61. ©2007, with permission from Elsevier.)

2.1.3.2 Cyclic Voltammetry

Cyclic voltammetry is the most useful technique in electrochemistry. It can quickly provide qualitative information about catalysts and electrochemical reactions, such as the electrochemical response of catalysts and the catalytic activity of the catalysts with respect to some electrochemical reactions. The principles of this technique have been discussed in detail in other chapters. Here, we simply look at the application of the technique in ORR catalyzed by surface adsorbed catalysts.

Figure 2.2 shows the cyclic voltammogram of an FePcCl_{16} adsorbed graphite electrode in 0.1 M H_2SO_4 solution. In the potential range of 1.15 V to -0.15 V , four waves (from high to low potential) – attributed to the redox pairs of $\text{Fe(IV)}/\text{Fe(III)}$, $\text{Fe(III)}/\text{Fe(II)}$, $\text{Fe(II)}/\text{Fe(I)}$, and the macrocyclic ring redox pair, respectively – can be observed [9, 10].

The peak currents of the wave of $\text{Fe(III)}/\text{Fe(II)}$ increase linearly with the potential scan rate, which is a typical feature of the reaction of an electrode surface adsorbed redox couple. From the slope, the electron number can be calculated according to the following equation [3, 9]:

$$I_p = \frac{n_{\text{Fe}^{\text{III}}\text{PcCl}_{16}}^2 F^2}{4RT} A \nu \Gamma_{\text{Fe}^{\text{III}}\text{PcCl}_{16}} \quad (2.10)$$

where $n_{Fe^{III}PcCl_{16}}$ is the electron transfer number involved in the electrochemical reaction of $Fe^{III}PcCl_{16}$, A is the electrode area, v is the potential scan rate, and $\Gamma_{Fe^{III}PcCl_{16}}$ is the surface concentration of the adsorbed species. From the slope of I_p vs. v , the surface concentration of $FePcCl_{16}$ can be calculated.

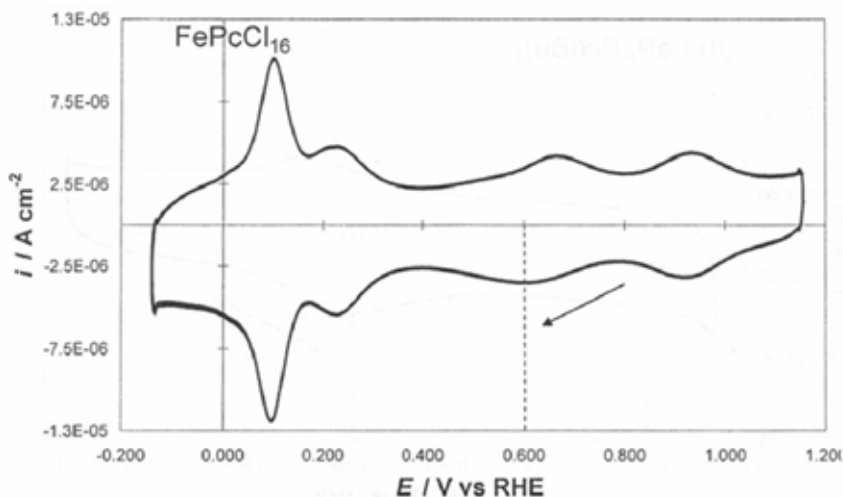
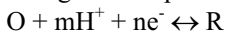


Figure 2.2. Cyclic voltammogram of $FePcCl_{16}$ adsorbed on a graphite electrode at 20 °C. Supporting electrolyte: 0.1 M H_2SO_4 . Potential scan rate: 100 $mV.s^{-1}$ [9]. (Reprinted from *Electrochimica Acta* (forthcoming), Baker R, Wilkinson DP, Zhang J. Electrocatalytic activity and stability of substituted iron phthalocyanines towards oxygen reduction evaluated at different temperatures. ©2008, with permission from Elsevier.)

The redox peak potential change that occurs with pH change sheds light on the electrochemical reaction mechanism of the surface adsorbed species. For a reaction involving either a proton or OH^- , e.g.,



the change in the formal potential (the average of the anodic potential and cathodic potential) vs. pH follows Equation 2.11:

$$E^f = E^0 - 2.303 \frac{mRT}{nF} pH \quad (2.11)$$

where E^f is the formal potential, E^0 is the Nernst potential, and the other terms have their usual significance [3, 10, 11].

In the case of $FePcCl_{16}$, as shown in Figure 2.2, the peak potential of $Fe(III)/Fe(II)$ as marked by the dotted line changes linearly with pH, and a slope of 56 $mV.pH^{-1}$ can be observed in the pH range of 0 to 14, which is reasonably close to a value of 58 $mV.pH^{-1}$ (20 °C), a theoretically expected value for a reversible reaction involving one electron and one proton [9, 10].

The onset potential and peak current demonstrate the catalytic activity of a catalyst. For example, CoHFPC has strong electrocatalytic activity towards oxygen reduction. Figure 2.3 compares the cyclic voltammograms of a bare graphite electrode (a) and a CoHFPC-coated graphite electrode (b) in air-saturated 0.1 M Na₂SO₄ solution. Both electrodes catalyze the O₂ reduction reaction, and the onset potential of ORR on the CoHFPC-coated electrode is 100–200 mV earlier than that of the bare graphite electrode [12].

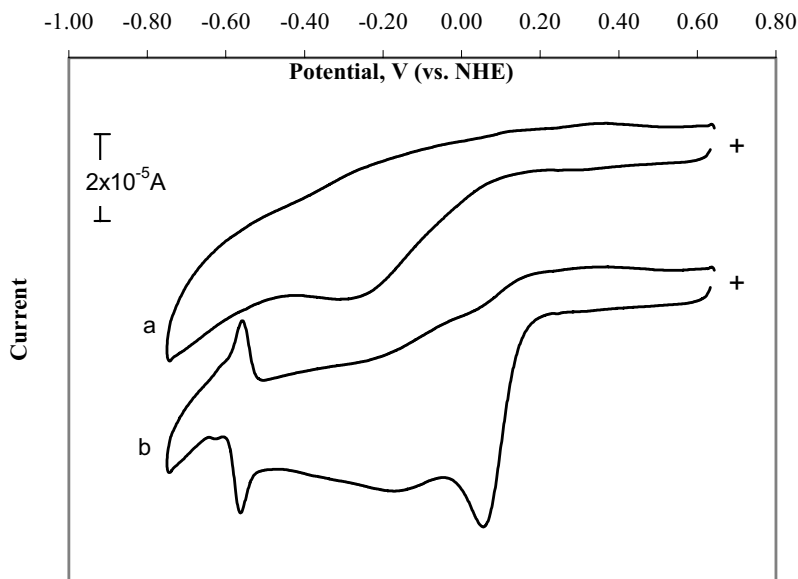


Figure 2.3. Cyclic voltammograms of (a) bare graphite electrode and (b) CoHFPC adsorbed graphite electrode, in air-saturated 0.1 M Na₂SO₄ buffered at pH 6. Potential scan rate: 100 mV.s⁻¹ [12]. (From Song C, Zhang L, Zhang J, Wilkinson DP, Baker R. Temperature dependence of oxygen reduction catalyzed by cobalt fluorophthalocyanine adsorbed on a graphite electrode. *Fuel Cells* 2007;7:9–15. ©2007 Wiley-VCH Verlag GmbH & Co. KGaA. Reproduced with permission.)

2.1.3.3 Rotating Disk Electrode

Equations used for RDEs are as follows [3]:

$$\frac{1}{I} = \frac{1}{I_k} + \frac{1}{I_{lev}} \quad (2.12)$$

(the Koutecky-Levich equation) where I is the disk current density, I_k is the kinetic current density, and I_{lev} is the Levich current density. I_k can be expressed as Equation 2.13:

$$I_k = nFAK_{O_2}C_{O_2}\Gamma_{catalyst} \quad (2.13)$$

where n is the overall electron transfer number, A is the electrode area, C_{O_2} is the concentration of dissolved O_2 , and Γ_{catalyst} is the surface concentration of the catalyst, or the catalyst loading. I_{lev} can be expressed as Equation 2.14:

$$I_{\text{lev}} = 0.201nFAC_{O_2}D_{O_2}^{\frac{2}{3}}\nu^{-\frac{1}{6}}\omega^{\frac{1}{2}} \quad (2.14)$$

where D_{O_2} is the diffusion coefficient of O_2 , ν is the kinematic viscosity of the electrolyte solution, and ω is the rotation rate represented by rpm.

An example of RDE application in ORR is shown in Figures 2.4 and 2.5. Figure 2.4 shows the RDE results obtained with a 5,10,15,20-Tetrakis (pentafluorophenyl)-21H,23H-porphine iron (III) (abbreviated as Fe^{III} TPFPP) coated graphite electrode in air-saturated 0.1 M H_2SO_4 solution. Figure 2.5 shows the Koutecky-Levich plot using results obtained from Figure 2.4. The slope of the Koutecky-Levich plot is the same as that of a 4-electron ORR theoretical line, meaning that the Fe^{III} TPFPP can catalyze a 4-electron oxygen reduction reaction. The Fe^{III} TPFPP-catalyzed ORR reaction constant was calculated to be $3.8 \times 10^8 \text{ mol}^{-1} \cdot \text{cm}^3 \cdot \text{s}^{-1}$ [11].

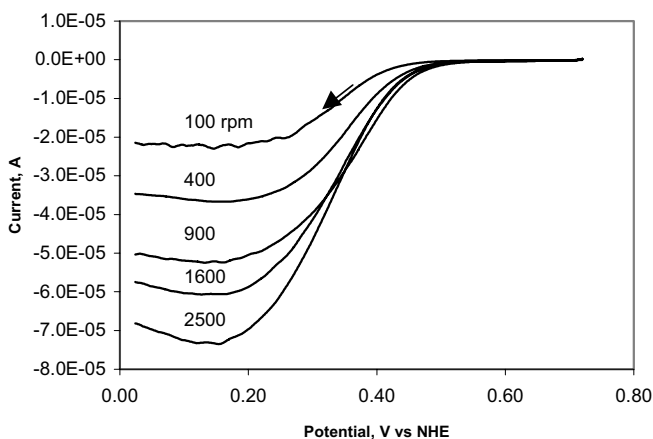


Figure 2.4. Current-potential curves for Fe^{III} TPFPP adsorbed on a rotating graphite disk electrode with different rotating rates, as marked on each trace, recorded in a 0.5 M H_2SO_4 air-saturated solution at 55 °C [11]. (Reproduced by permission of ECS—The Electrochemical Society, from Zhang L, Song C, Zhang J, Wang H, Wilkinson DP. Temperature and pH dependent oxygen reduction catalyzed by iron fluoro-porphyrin adsorbed on a graphite electrode.)

For RDE data analysis, three non-electrochemical kinetic parameters, such as the diffusion coefficient of O_2 , the kinematic viscosity of the electrolyte solution, and the solubility of O_2 must be known accurately. These parameters are all temperature dependent. Their values are also slightly dependent on the electrolyte used. Table 2.3 lists these parameters at various conditions.

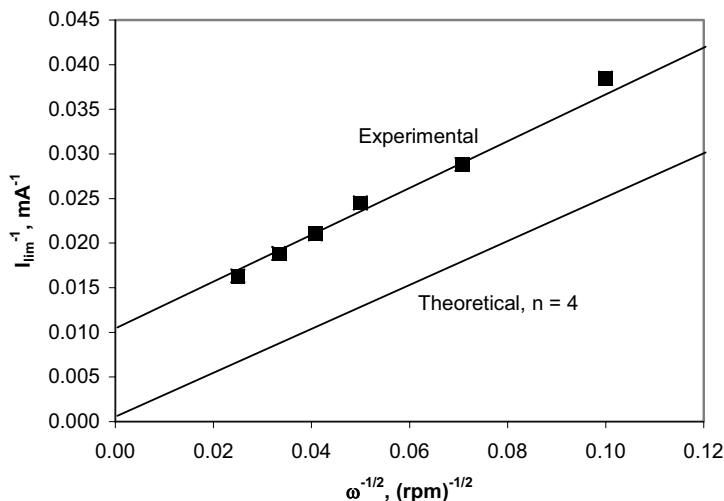


Figure 2.5. Koutecky-Levich plot using data from Figure 2.4. The theoretical line is calculated according to Levich theory for a 4-electron O_2 reduction process [11]. (Reproduced by permission of ECS—The Electrochemical Society, from Zhang L, Song C, Zhang J, Wang H, Wilkinson DP. Temperature and pH dependent oxygen reduction catalyzed by iron fluoro-porphyrin adsorbed on a graphite electrode.)

Table 2.3. Non-electrochemical kinetic parameters for RDE data analysis

Experiment conditions (T, P, electrolyte)	Diffusion coefficient of O_2 , $\text{cm}^2.\text{s}^{-1}$	Kinematic viscosity of the electrolyte solution, $\text{cm}^2.\text{s}^{-1}$	Solubility of O_2 , $\text{mol}.\text{cm}^{-3}$	Ref.
0.1 M HClO_4 , 20°C, 1 atm O_2	1.67×10^{-5}	-	1.38×10^{-6}	8
0.5 M H_2SO_4 , 25°C, 1 atm O_2	1.4×10^{-5}	0.010	1.1×10^{-6}	68
0.1 M KOH , 25°C, 1 atm O_2	1.9×10^{-5}	-	1.2×10^{-6}	7
1 M NaOH , 25°C, 1 atm O_2	1.65×10^{-5}	0.011	8.4×10^{-7}	15
0.1 M TBAP quinoline, 25°C, 1 atm O_2	1.71×10^{-5}	0.033	1.49×10^{-6}	92

2.1.3.4 Rotating Ring-disk Electrode (RRDE)

In the RRDE method, the O_2 reduction reaction occurring on the disk electrode produces intermediates, which can be detected on the ring and are used to deduce the ORR mechanism. An example is using RRDE to study the O_2 reduction reaction catalyzed by Pt/C catalysts with different particle sizes. On the disk, 2-

electron and 4-electron ORR can occur, and on the ring electrode, H_2O_2 is further oxidized to H_2O [13].

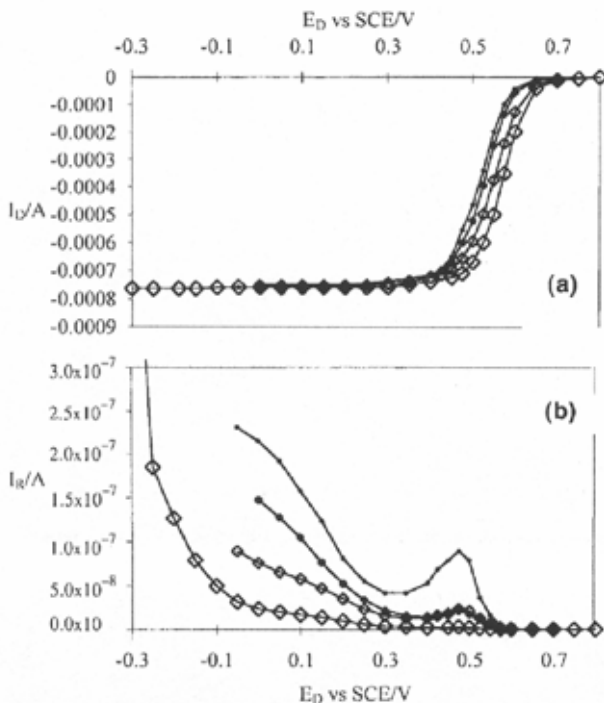


Figure 2.6. Oxygen reduction current (a) on a disk electrode for active layers with different Pt mass ratios Pt/(Pt+C) and H_2O_2 oxidation curves, (b) on the ring electrode (1 mV s^{-1} ; $0.1 \text{ M H}_2\text{SO}_4$; 293 K ; $L \approx 3 \text{ }\mu\text{m}$; Nafion/carbon volume ratio = 1; 10% Pt/(Pt+C): (\diamond) $d = 2.5 \text{ nm}$, $S_{\text{Pt}} = 7.6 \text{ cm}^2$; 20%: (\diamond) $d = 3.4 \text{ nm}$, $S_{\text{Pt}} = 13.9 \text{ cm}^2$; 30%: (\diamond) $d = 4.1 \text{ nm}$, $S_{\text{Pt}} = 19.4 \text{ cm}^2$; 40%: (\diamond) $d = 5.1 \text{ nm}$, $S_{\text{Pt}} = 24.3 \text{ cm}^2$) [13]. (With kind permission from Springer Science+Business Media: Journal of Applied Electrochemistry, RRDE study of oxygen reduction on Pt nanoparticles inside Nafion®: H_2O_2 production in PEMFC cathode conditions, 30, 2004, 839–844, O. Antoine, Figure 1, ©2004 Springer.)

The 2-electron reduction current (I_{2e^-}) is given by

$$I_{2e^-} = I_R / N \quad (2.15)$$

where I_{2e^-} is the 2-electron ORR on the disk electrode and N is the collecting coefficient number. The ORR current (I_D) on disk electrode can be expressed as Equation 2.16:

$$I_D = I_{2e^-} + I_{4e^-} \quad (2.16)$$

where I_{4e^-} is the 4-electron ORR current. The following equation is used to obtain the average electron number (n_{e^-}) involved in ORR:

$$\frac{I_D}{n_{e^-}} = \frac{I_{4e^-}}{4} + \frac{I_{2e^-}}{2} \quad (2.17)$$

By rearranging Equation 2.17, we get Equation 2.18, which is used to calculate n_{e^-} :

$$n_{e^-} = \frac{4I_D}{I_D + I_R / N} \quad (2.18)$$

Figure 2.6 shows the ring-disk currents of ORR on different Pt/C catalyst with different particle sizes. Figure 2.7 shows the average electron transfer numbers calculated based on Equation 2.18. The numbers are close to 4 for all catalysts investigated, indicating a weak platinum particle size effect on H_2O_2 production. Larger particle size shows a higher proportion of H_2O_2 .

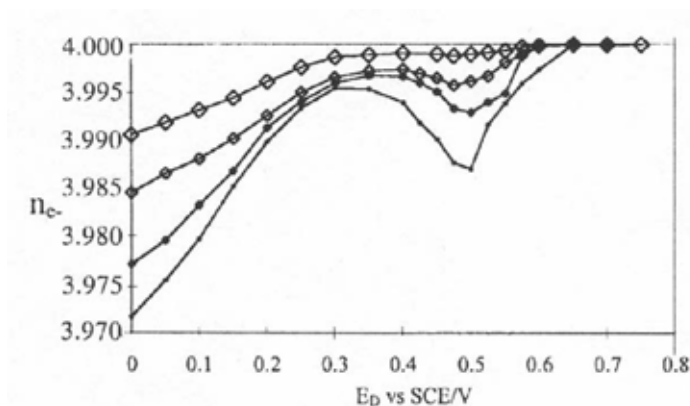


Figure 2.7. Average number of exchanged electrons during oxygen reduction on the disk active layer. Data obtained based on Figure 2.6 [13]. (10% Pt/(Pt+C): (\diamond) $d = 2.5$ nm, $S_{Pt} = 7.6$ cm²; 20%: (\diamond) $d = 3.4$ nm, $S_{Pt} = 13.9$ cm²; 30%: (\diamond) $d = 4.1$ nm, $S_{Pt} = 19.4$ cm²; 40%: (\diamond) $d = 5.1$ nm, $S_{Pt} = 24.3$ cm²). (With kind permission from Springer Science+Business Media: Journal of Applied Electrochemistry, RRDE study of oxygen reduction on Pt nanoparticles inside Nafion®: H_2O_2 production in PEMFC cathode conditions, 30, 2004, 839–844, O. Antoine, Figure 2, ©2004 Springer.)

2.2 Oxygen Reduction on Graphite and Carbon

It seems that all carbon materials have some electrocatalytic activity towards ORR in alkaline solutions [2]. The materials that have been studied include graphite,

glassy carbon, active carbon, and carbon nanotubes [2, 14–22]. Depending on the type of carbon, the catalytic ORR activity and mechanism vary widely. For example, glassy carbon and pyrolytic graphite normally catalyze a 2-electron transfer oxygen reduction, producing H_2O_2 . On an oxidized glassy carbon electrode [14] and oxidized graphite electrodes [15], the H_2O_2 can be further reduced to water at more negative potentials. On carbon nanotubes [16], the O_2 reduction product is H_2O_2 or a mixture of H_2O_2 and OH^- , depending on the preparation method and potential of the carbon nanotube-modified electrode.

2.2.1 Oxygen Reduction Reaction Mechanisms

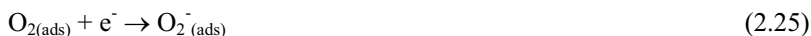
2.2.1.1 ORR on Graphite and Glassy Carbon

Two mechanisms have been proposed for carbon-catalyzed ORR. On a glassy carbon electrode, the following reaction mechanism has been proposed [2]:



The subscripts “ads” indicate the corresponding species are adsorbed on the electrode surface. The reactant and product in Reaction 2.21 are two different forms of the superoxide ion on the carbon surface. The left one is a relatively inert form adsorbed on an inert graphite site, and the right one is the same species, but migrating to an active site according to Reaction 2.21. It was confirmed that Reaction 2.21 was the rate determining step. However, Taylor et al. [14, 17] found that the rate determining step was dependent on pH. At $\text{pH} > 10$, Reaction 2.21 was the rate determining step, and at $\text{pH} < 10$, Reaction 2.20 was the rate determining step.

On pyrolytic graphite electrodes, the first reaction was also proposed as Reaction 2.19, followed by:



and the rate determining step was believed to be Reaction 2.25.

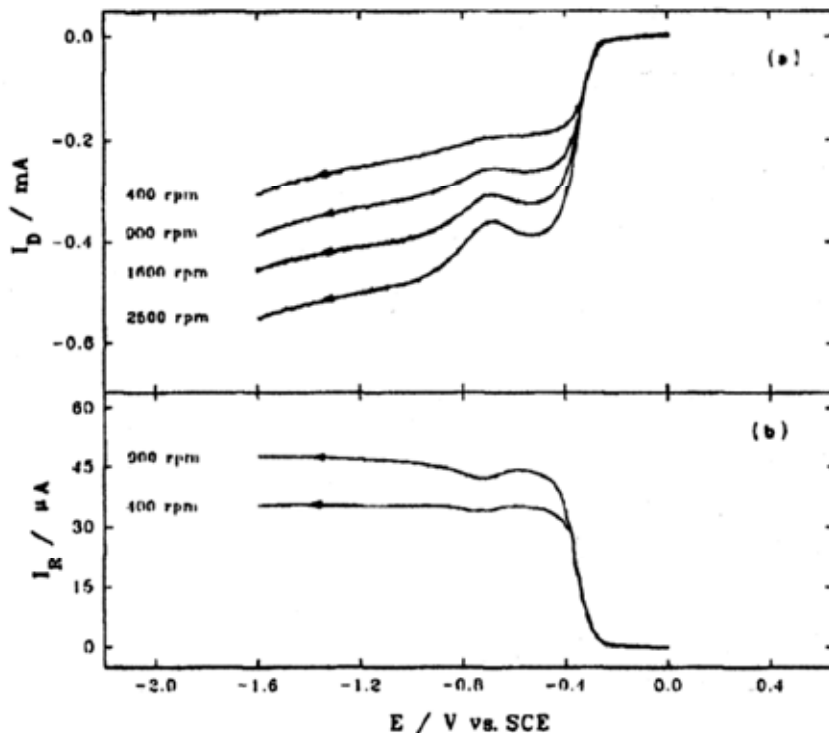


Figure 2.8. (a) Current-potential curves for O_2 -saturated 1.0 M NaOH solution at a polished glassy carbon disk electrode, $T = 298$ K. Potential scan rate: 5 mV/s; (b) response at a Pt ring held at 0.0 V vs. SCE during the potential scan at the disk. Rotation rates are given on the figure [21]. (Reprinted from Journal of Electroanalytical Chemistry, 382(1–2), Baez Victor B. and Pletcher Derek, Preparation and characterization of carbon/titanium dioxide surfaces—the reduction of oxygen, 59–64, ©1995, with permission from Elsevier.)

For ORR current-potential curves recorded on either a graphite or a glassy carbon electrode surface, two waves were observed, both of which were attributed to the 2-electron transfer reduction of O_2 , producing H_2O_2 . Figure 2.8 shows the RRDE results for O_2 reduction on a glassy carbon electrode. On the disk electrode, the first steep wave appears at the formal potential ($E_{1/2}$) of -0.34 V vs. SCE and the second one at $E_{1/2} = -0.78$ V. The oxidation current at the ring shows that both waves correspond to H_2O_2 production. This 2-electron reduction occurs at two different potential ranges, suggesting that there are two kinds of ORR active sites on glassy carbon. In a further experiment with 1 M NaOH solution containing 5 mM H_2O_2 , no reduction wave was observed. This result confirmed that H_2O_2 could not be further reduced on a glassy carbon electrode [21].

The ORR activity of a graphite electrode is dependent on graphite planes. The activity on an edge plane is higher than that on a basal plane, as shown in Figure 2.9 [22]. This reflects the difference in electrocatalytic activity of these two orientations. This catalytic activity difference is mainly due to there being more functional groups on an edge plane than on a basal plane.

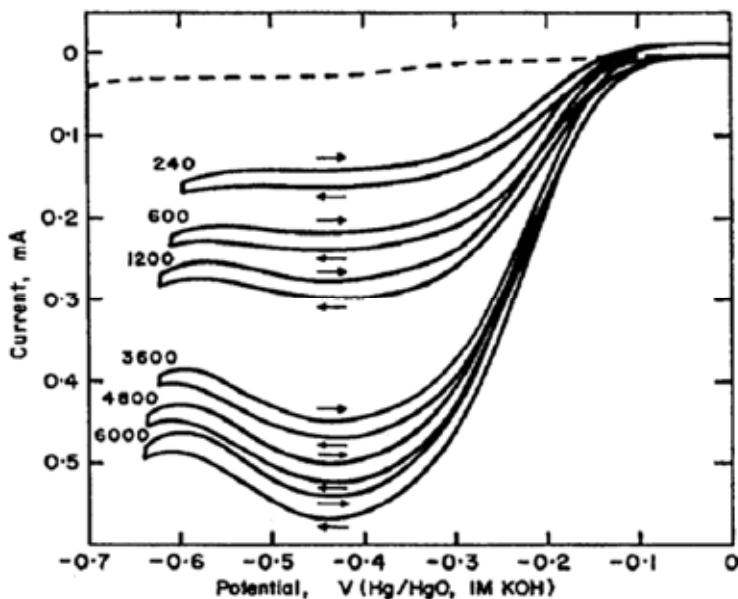


Figure 2.9. Current-potential curves for O_2 -saturated 1 M KOH solution on high pressure annealed pyrolytic graphite: — edge plane, --- basal plane [22]. (Reprinted from *Electrochimica Acta*, 15(6), Morcos I. and Yeager E., Kinetic studies of the oxygen—peroxide couple on pyrolytic graphite, 953–75, ©1970, with permission from Elsevier.)

2.2.1.2. ORR on Carbon Nanotubes

Carbon nanotubes are a new kind of material with extensive applications. Recently, oxygen reduction reaction catalyzed by carbon nanotubes has been investigated by several groups [16, 20], which found that the catalyzed ORR was dependent on the preparation method for the carbon nanotube films. Zhang et al. [16] prepared multiwalled carbon nanotube (MWCNT) films by a dihexadecyl hydrogen phosphate (DHP) method on a glassy carbon electrode and found that the films could catalyze O_2 reduction by two 2-electron processes, producing OH^- . At a potential range of -0.4 – -0.8 V vs. Ag/AgCl, the first reduction current plateau was observed, and was attributed to a 2-electron process producing H_2O_2 . At potentials more negative than -0.9 V, a second plateau appeared, which was attributed to the further reduction of H_2O_2 , producing OH^- (see curve 1' in Figure 2.10). Jurmann et al. [20] prepared similar films using the same method on a highly oriented pyrolytic graphite electrode, and reported that the first 2-electron process could be observed at the potential range of -0.4 – -0.6 V vs. SCE, while the second plateau was not clearly discerned. A mixture process of 2- and 4-electron reduction could be observed at more negative potentials. Jurmann et al. [20] also found that on MWCNT films prepared by the poly(diallyldimethylammonium chloride) method, the electron transfer number of ORR was in the range of 3 – 3.5 at the potential range of -0.4 – -1.2 V. Figure 2.10 shows the results, together with those obtained on a bare glassy carbon electrode for comparison. It can be seen that on a glassy carbon electrode, the ring

current increases as disk current increases in the potential range of -0.4 to -1.2 V. However, on an MWCNT-modified electrode, the ring current decreases as the disk current increases in the similar potential range, indicating less H_2O_2 is produced.

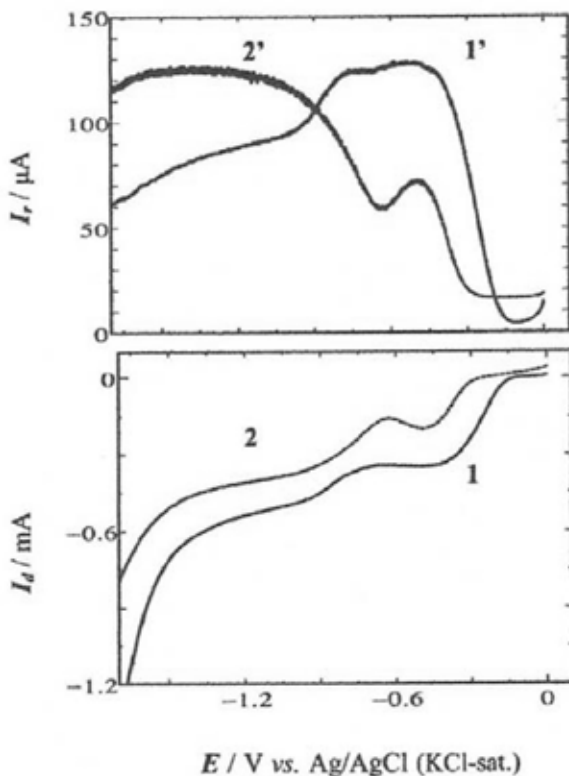


Figure 2.10. RRDE voltammograms for O_2 reduction at the PDDA/MWCNTs/GC (curve 1) and bare GC (curve 2) disk electrodes in O_2 -saturated 0.10 M KOH solution. Curves 1' and 2' represent the current for the oxidation of HO_2^- produced at the corresponding disk electrodes. Potential scan rate: 10 mV/s; electrode rotating rate: 400 rpm. The Pt ring electrode was polarized at +0.50 V for the oxidation of HO_2^- [16]. (Reprinted with permission from Langmuir 2004;20;8781–5. Copyright 2004 American Chemical Society.)

2.2.1.3. ORR on Heteroatom Doped Carbons

Doping carbon with heteroatoms such as nitrogen can change the carbon's properties. For example, nitrogen (N)-doped carbon shows high oxidation resistance capability and higher catalytic activity toward ORR. Maldonado and Stevenson [23] found that N-doped carbon fiber showed improved catalytic activity by shifting the ORR potential up by 70 mV (Figure 2.11), and the electron transfer number of ORR catalyzed by N-doped carbon fiber was close to 4. They discussed that N-doped carbon can not only catalyze O_2 reduction reaction but also catalyze H_2O_2 decomposition [23].

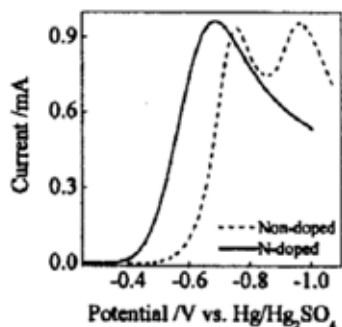


Figure 2.11. Background subtracted voltammetric responses of a nondoped CNF electrode (dashed line) and an N-doped CNF electrode (solid line) immersed in an O_2 -saturated 1 M KNO_3 solution. Scan rate = 0.1 V s^{-1} [23]. (Reprinted with permission from J Phys Chem B 2005;109.10:4707–16. Copyright 2005 American Chemical Society.)

The active sites in N-doped carbon are carbon atoms adjacent to the N atom. Using a cluster model, Sidik et al. [24] did theoretical calculations and found that carbon radical sites adjacent to the substitutional N showed strong bonding ability to adsorbed OOH, favoring the production of H_2O_2 [24], which improves its catalytic activity.

2.2.1.4 ORR on Pre-treated Carbon Surface

Pre-treatment of carbon materials can significantly improve their catalytic activity towards ORR and change their electrochemical behavior. A variety of treatment methods have been used, including polishing the electrode, radio frequency plasma treatment, heating at low pressures, *in situ* laser irradiation, vacuum heat treatment, chemical oxidation, and electrochemical oxidation [25–28].

It is not clearly understood why pre-treatment of carbon surfaces improves their catalytic activity. Pre-treatment does create more surface functional groups, and exposes fresh carbon edges, microparticles, and defects [25–27]. Jia et al. [28] found that pre-treatment of carbon supports and Pt-loaded carbon supports resulted in ionic resistance decrease, indicating that surface functional groups such as carboxylic acid were generated. Pre-treatment also might increase the surface area of carbon by generating porous surface films [29]. Sullivan et al. [29] found that surface oxidation of glassy carbon at 1.95 V vs. SCE leads to the formation of porous carbon film, and that the film thickness increased linearly with oxidation time. Overall, pre-treatment of carbon can change its surface state. The surface groups or changed surface state facilitate ORR by acting as an electron transfer mediator or by increasing adsorption sites for O_2^- species, which enhances the kinetics of ORR.

Figure 2.12 shows the current-potential curves of an unoxidized glassy carbon electrode that had then been oxidized at 2 V vs. RHE in 0.5 M H_2SO_4 at different times. Increasing the oxidation time resulted in decreased ORR onset potential and increased ORR reduction current.

Pretreated carbon also affects the activity of other catalysts supported on it. For example, pretreatment of a carbon support followed by deposition of Pt on it and

treatment of carbon-supported Pt also resulted in significant increases in the ORR catalytic activity of Pt. Jia et al. [28] reported that an untreated catalyst (Pt deposited on untreated carbon supports) gave a kinetic current of 0.3 ± 0.1 mA at 0.6 V vs. SCE, while Pt deposited on pretreated carbon showed a kinetic current of 1.6 ± 0.7 mA, and posttreated carbon-supported Pt catalyst (refluxing carbon-supported Pt catalyst in nitric acid) could give a kinetic current of 7.7 ± 1.7 mA.

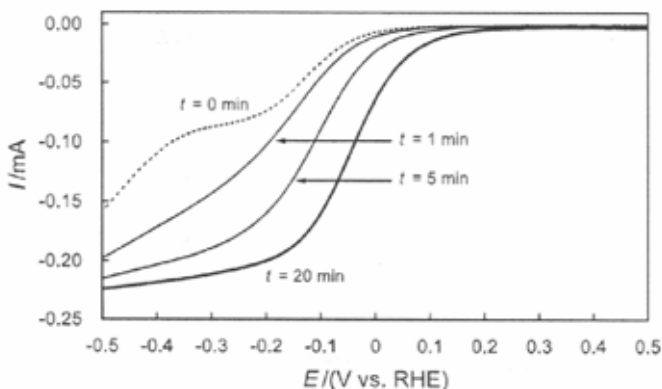


Figure 2.12. Hydrodynamic voltammograms for O_2 reduction at a bare glassy carbon RDE in O_2 -saturated 0.5 M H_2SO_4 . Glassy carbon surface oxidation time: 0 min (dashed line); 1 min (thin line); 5 min (thick line); 20 min (very thick line). Scan rate: 10 mV/s; rotation speed: 2000 rpm [27]. (Reprinted from Journal of Electroanalytical Chemistry, 527(1–2), Maruyama J, Abe I, Cathodic oxygen reduction at the interface between Nafion® and electrochemically oxidized glassy carbon surfaces, 65–70, ©2002, with permission from Elsevier.)

2.2.2 Kinetics of the ORR on Carbon Materials

On a glassy carbon electrode, the Tafel slope was observed to be 60 mV/dec in alkaline solutions, and at pH < 10, the Tafel slope was 120 mV/dec. These values are in accordance with the proposed mechanisms. In the case of 120 mV/dec, the first electron transfer is the rate determining step. In the case of 60 mV/dec, the current-potential relationship observed from the multiple-electron transfer process of ORR on carbon electrodes was expressed as Equation 2.27, given by Taylor and Humffray [14, 17]:

$$i = i_0 \left\{ \exp \left[\frac{n-\gamma}{\nu} - r\beta \right] \frac{F\eta}{RT} \right\} - \exp \left[- \left(\frac{\gamma}{\nu} + r\beta \right) \frac{F\eta}{RT} \right] \quad (2.27)$$

where η is the overpotential, γ is the number of electrons transferred before the rate determining step (rds), n is the number of electrons involved in the overall reaction, β is the symmetry factor of the rds, r is the number of electrons transferred in the rds if the rds involves charge transfer (if no electron transfer is involved in the rds, $r = 0$), and ν is the stoichiometric number of the reaction.

The stoichiometric number ν was evaluated from the current-potential measurements in the region of low overpotential, according to the following relation:

$$\left(\frac{\partial \eta}{\partial i}\right)_{i \rightarrow 0} = \frac{\nu RT}{nF i_0} \quad (2.28)$$

On carbon materials, ν usually equals 1. Using Allen and Hickling's graphical treatment, Taylor and Humffray found that the Tafel slope is $2.303 \frac{RT}{(\frac{\gamma}{\nu} + r\beta)F}$ and

that its numerical value is 60 mV/dec. This indicates that $\gamma = 1$ and $r = 0$, meaning that the migration step is the rds.

2.2.3 Catalytic Sites on Carbon Materials

The catalytic ORR activity of carbon materials is generally attributed to the quinone groups [2]. Yeager [2] cited Garten and Weiss's mechanism for O_2 reduction on carbon surfaces, as shown in Figure 2.13. A similar mechanism was also proposed for a carbon nanotube surface, as in Figure 2.14 [16]. Although this mechanism has not been confirmed, electrodes modified with a variety of quinone compounds have shown great catalytic activity towards 2-electron oxygen reduction reaction for H_2O_2 production (see Section 2.3).

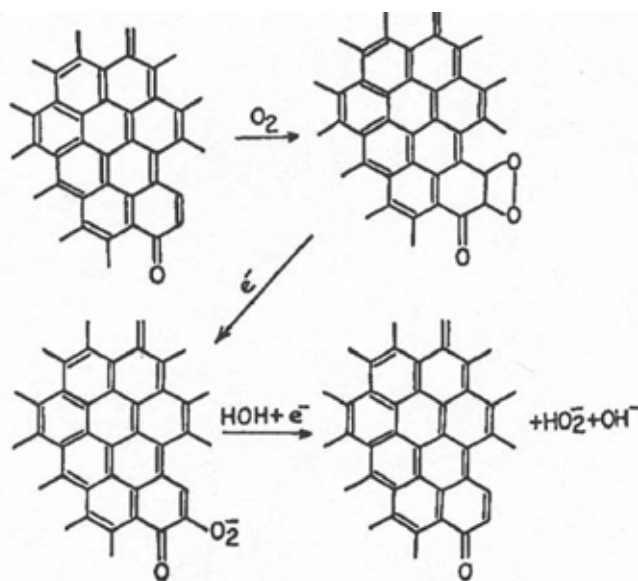


Figure 2.13. Garten and Weiss's mechanism for reduction on carbon surface [2]. (Reprinted from Journal of Molecular Catalysis, 38(1–2), Yeager Ernest, Dioxygen electrocatalysis: mechanisms in relation to catalyst structure, 5–25, ©1986, with permission from Elsevier.)

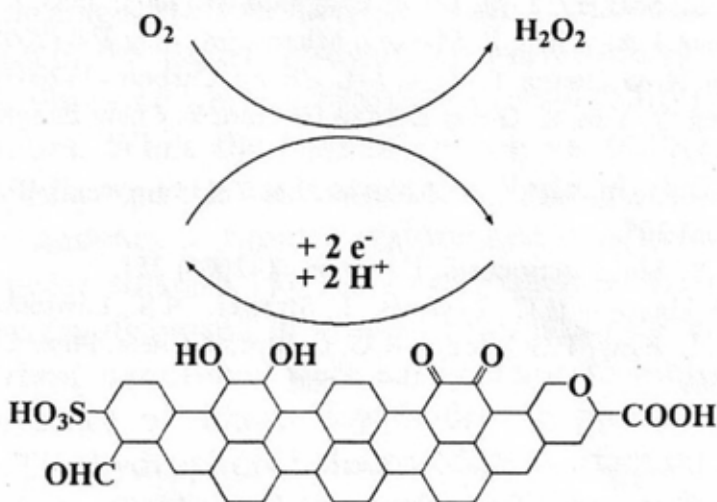


Figure 2.14. Mechanism of O_2 reduction on carbon nanotube surface [20]. (Reprinted from Journal of Electroanalytical Chemistry, 597(2), Jürmann Gea and Tammeveski Kaido, Electroreduction of oxygen on multi-walled carbon nanotubes modified highly oriented pyrolytic graphite electrodes in alkaline solution, 119–26, ©2006, with permission from Elsevier.)

2.3 Oxygen Reduction Catalyzed by Quinone and Derivatives

As discussed above, the surface quinone group on a carbon electrode can catalyze a 2-electron O_2 reduction reaction, producing H_2O_2 . This ORR process has attracted significant attention in terms of fundamental understanding and applications [30–41].

2.3.1 AO Process for O_2 Reduction to Produce H_2O_2

H_2O_2 , a product of the 2-electron transfer reduction of O_2 , has wide industrial applications, including pulp and paper, textiles, chemical synthesis, as well as environmental protection such as waste-water treatment. The most commonly used industrial production procedure is the anthraquinone process, or “AO process”. The chemical reaction involved in the process is expressed in Figure 2.15.

The catalyst used in this process is Raney Ni, or Pd/Al_2O_3 . Anthraquinone dissolved in a solvent mixture was hydrogenated by the catalyst, then oxidized with air. By this method, H_2O_2 can be produced and the starting material, anthraquinone, recovered [31]. In the process, anthraquinone degradation is a problem and results in decreased efficiency. Researchers are therefore trying to replace the chemical reduction step of anthraquinone with electrochemical reduction [30, 32, 33].

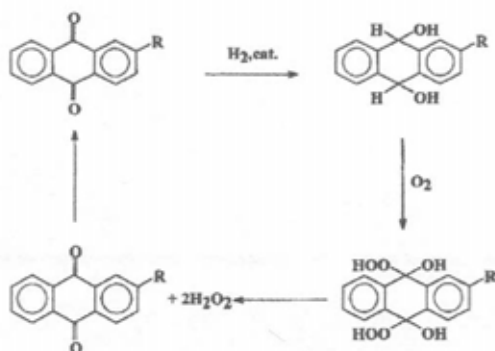
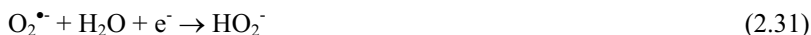
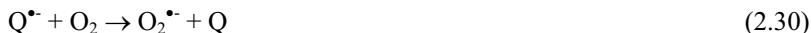


Figure 2.15. The anthraquinone process (AO process) to produce H_2O_2 [30]. (With kind permission from Springer Science+Business Media: Journal of Applied Electrochemistry, Electrochemical reduction of 2-ethyl-9,10-anthraquinone (EAQ) and mediated formation of hydrogen peroxide in a two-phase medium Part I: Electrochemical behaviour of EAQ on a vitreous carbon rotating disc electrode (RDE) in the two-phase medium, 29, 2004, 11–16, A. Huissoud, Scheme 1, ©Springer.)

2.3.2 ORR Mechanism Electrochemically Catalyzed by Quinone

The O_2 reduction of O_2 catalyzed by the quinone group is proposed to proceed by the following electrochemical-chemical (EC) process [30, 37]:



or



where Q represents the quinone group. Reaction 2.30 was considered to be the rate determining step. Quinones with different substituted groups, such as ethyl group modified anthraquinones, were also investigated in order to improve the catalytic activity and stability [38].

2.4 Oxygen Reduction on Metal Catalysts

2.4.1 ORR Mechanism on Pt

Oxygen reduction reaction on a Pt electrode has been the most extensively studied mechanism. This catalytic ORR is a multi-electron process with a number of

elementary steps, involving different reaction intermediates. The simplified version of the mechanism is shown in Figure 2.16; the only two products are H_2O_2 and H_2O . RRDE measurements show that on a Pt surface, O_2 reduction is a major 4-electron transfer process from O_2 to H_2O in both acid and alkaline aqueous electrolytes if adsorbed impurities are absent [42]. At this point, the mechanism of ORR on Pt is still not well understood.

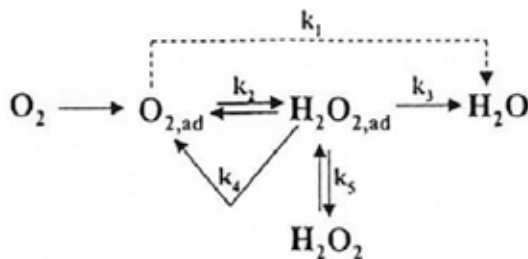


Figure 2.16. The oxygen reduction reaction mechanism on Pt [42]. (Reprinted from Surface Science Reports, 45(4–6), Markovi N. M. and Ross P. N., Surface science studies of model fuel cell electrocatalysts, 117–229, ©2002, with permission from Elsevier.)

The mechanism shown in Figure 2.16 indicates that O_2 can be reduced either directly to water (direct 4-electron reduction) electrochemically with the rate constant k_1 , or to adsorbed hydrogen peroxide ($\text{H}_2\text{O}_{2,\text{ad}}$) with the rate constant k_2 (“series” 2-electron reduction). $\text{H}_2\text{O}_{2,\text{ad}}$ can be further reduced to water with the rate constant k_3 , chemically decomposed on the electrode surface (k_4), and/or desorbed into the electrolyte solution (k_5). Some experimental results suggest that a series pathway via an $(\text{H}_2\text{O}_2)_{\text{ad}}$ intermediate is the most possible pathway. For example, only a very small amount of H_2O_2 could be observed during ORR, and the electron transfer number is close to 4. This series ORR mechanism suggests a special case of $k_1 = 0$.

The ORR mechanism on Pt has also been investigated by theoretical calculation based on the electronic structure, using density functional theory [43–45]. The dissociative mechanism and the associative mechanism are proposed for a low current density range and a high current density range, respectively [43, 44]:

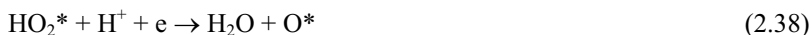
(1) *Dissociative Mechanism:*



where $*$ denotes a site on the Pt surface. In this mechanism, no H_2O_2 is produced. On a Pt surface, O_2 adsorption breaks the O–O bond and forms adsorbed atomic O, which further gains two electrons in the two consecutive steps, forming water.

Since there is no adsorbed O_2 on the Pt surface, H_2O_2 cannot be formed. This mechanism can be considered a detailed form of the direct 4-electron pathway.

(2) *Associative Mechanism:*

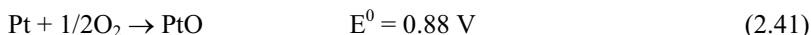


This mechanism also does not involve H_2O_2 . Since adsorbed O_2 is present, the O-O bond may not be broken in the following steps, resulting in the formation of H_2O_2 . The H_2O_2 could either be further reduced to H_2O or be a final product. Therefore, this mechanism might be an alternative expression of that in Figure 2.16.

2.4.2 Mixed Pt Surface and Rest Potential on Pt

The thermodynamic potential of ORR (1.23 V vs. NHE at standard conditions) is so high that no electrode materials can remain pure. At 1.23 V, electrode materials undergo oxidation, which changes their surface properties.

On Pt and at high potential, the following reaction occurs:



Thus, in the presence of O_2 , the Pt surface is a mixture of Pt and PtO. Therefore, a steady-state open circuit potential (OCP) of 1.23 V is rarely observed, due to the formation of PtO. Rather, the steady-state rest potential of a Pt electrode in O_2 saturate 1 M H_2SO_4 is 1.06 V, a mixed value of the thermodynamic potential of O_2/H_2O and of Pt/PtO, because two reactions occur: Pt oxidation and O_2 reduction [46].

For Pt oxidation, the oxidation current-overpotential relationship is given by

$$I_{Pt/PtO} = i_{Pt/PtO}^0 \left(e^{\frac{n_{\alpha,Pt/PtO} \alpha_{\alpha,Pt/PtO} F \eta_{Pt/PtO}}{RT}} - e^{\frac{n_{\alpha,Pt/PtO} (1-\alpha_{\alpha,Pt/PtO}) F \eta_{Pt/PtO}}{RT}} \right) \quad (2.42)$$

where $I_{Pt/PtO}$ is the Pt oxidation current, $i_{Pt/PtO}^0$ is the exchange current density of Pt oxidation, $n_{\alpha,Pt/PtO}$ is the apparent electron transfer number in the electrochemical reaction, $\alpha_{\alpha,Pt/PtO}$ is the electron transfer coefficient, and

$\eta_{a,Pt/PtO} = E^{rest} - 0.88$ is the overpotential (E^{rest} is the steady-state rest potential of the system).

Assuming the overpotential is small, this equation can be approximated as follows:

$$I_{Pt/PtO} = i_{Pt/PtO}^o \frac{n_{\alpha,Pt/PtO} F}{RT} (E^{rest} - 0.88) \quad (2.43)$$

For the O_2 reduction reaction on Pt, a similar equation can be written as:

$$I_{O_2/H_2O} = i_{O_2/H_2O}^o \frac{n_{\alpha,O_2/H_2O} F}{RT} (1.23 - E^{rest}) \quad (2.44)$$

where I_{O_2/H_2O} is the O_2 reduction current, i_{O_2/H_2O}^o is the exchange current density of O_2 reduction, $n_{\alpha,O_2/H_2O}$ is the apparent electron transfer number in the electrochemical reaction, $\alpha_{\alpha,O_2/H_2O}$ is the electron transfer coefficient, and $E^{rest} - 0.88$ is the overpotential.

Since no net current is flowing from the system or given to the system, $I_{Pt/PtO} = I_{O_2/H_2O}$. Thus,

$$n_{\alpha,Pt/PtO} i_{Pt/PtO}^o (E^{rest} - 0.88) = n_{\alpha,O_2/H_2O} i_{O_2/H_2O}^o (1.23 - E^{rest}) \quad (2.45)$$

Assuming the exchange current density and apparent electron transfer number for Pt oxidation and O_2 reduction are the same, the value of E^{rest} can be obtained through Equation 2.45, and is 1.06 V. However, the value of this rest potential can be changed by altering the extent to which PtO covers the electrode surface.

2.4.3 ORR Kinetics on Pt

The electrode potential can play a significant role in changing the Pt surface structure in the presence of O_2 , due to the mixed potential discussed above. At higher potentials (> 0.8 V), the electrode surface is a mixture of Pt and PtO, while at lower potentials, the Pt surface is pure Pt. Thus, the kinetics of O_2 reduction on Pt is not expected to be the same in different potential ranges. Figure 2.17 shows the two Tafel slopes observed for ORR on a Pt electrode surface [8]. At a low current density range (high potential), a Tafel slope of 60 mV/dec was obtained. At a high current density range (low potential), a value of 120 mV/dec was observed. The difference in Tafel slope indicates that the mechanism on a Pt/PtO surface is different from that on a pure Pt surface. On a Pt/PtO surface, the rate determining step is a pseudo 2-electron procedure, which gives a Tafel slope of 60 mV/dec. However, on a pure Pt surface, the first electron transfer is the rate determining step, resulting in a Tafel slope of 120 mV/dec.

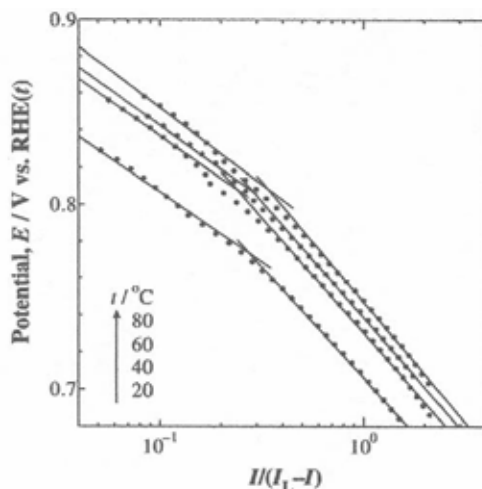


Figure 2.17. Tafel plots for oxygen reduction reaction at a Pt working electrode [8]. (Reprinted from Journal of Electroanalytical Chemistry, 574(2), Wakabayashi Noriaki, Takeichi Masayuki, Itagaki Masayuki, Uchida Hiroyuki and Watanabe Masahiro, Temperature-dependence of oxygen reduction activity at a platinum electrode in an acidic electrolyte solution investigated with a channel flow double electrode, 339–46, ©2005, with permission from Elsevier.)

Using a DFT model, Norskov et al. [44] calculated the dissociative mechanism and gave a Tafel slope of 60 mV/dec. Unfortunately, the literature does not devote enough attention to the associative mechanism.

The ORR exchange current density on a Pt electrode can be obtained by extrapolating the potential-log(*I*) plot along the Tafel line to the thermodynamic potential. Two Tafel slopes give two exchange current densities, one at a low current density (high potential), and the other in a high current density range (low potential). The values of the ORR exchange current densities on Pt vary widely in the literature, depending primarily on the morphology of the Pt catalyst. This can also be seen in Table 2.2. For example, Parthasarathy et al. [7] reported that the values on a Pt wire/Nafion membrane interface at 80 °C are 1.8×10^{-8} A/cm² at high potential range (low current density, with Tafel slope of 60 mV/dec) and 1.4×10^{-6} A/cm² at low potential range (high current density, with a Tafel slope of 120 mV/dec). Our recent study on the kinetics of ORR in PEM fuel cells showed that at 80 °C, the exchange current density is 6.25×10^{-6} at high potential range (low current density) and 3.87×10^{-4} A/cm² at low potential range (high current density), respectively [4]. For the catalyst, we used Pt nanoparticles supported on Vulcan carbon.

2.4.4 ORR on Pt Alloys

The catalytic activity of Pt towards ORR strongly depends on its O₂ adsorption energy, the dissociation energy of the O-O bond, and the binding energy of OH on the Pt surface. The electronic structure of the Pt catalyst (Pt *d*-band vacancy) and

the Pt-Pt interatomic distance (geometric effect) can strongly affect these energies [47]. Theoretical calculations on O_2 and OH binding energy on several metals have predicted that Pt should have the highest catalytic activity among other metals with the ORR activity of $Pt > Pd > Ir > Rh$, which is in agreement with the experimental results. Regarding the Pt alloy catalysts, calculations have also predicted that PtM (M=Fe, Co, Ni, etc.) alloys should have higher catalytic activity than pure Pt, which has again been proven by experiments [44].

The activity enhancement that occurs when Pt is alloyed with other metals is explainable by the change in electronic structure (the increased Pt d -band vacancy) and in geometric effect (Pt-Pt interatomic distance). Alloying causes a lattice contraction, leading to a more favorable Pt-Pt distance for the dissociative adsorption of O_2 . The d -band vacancy can be increased after alloying, producing a strong metal- O_2 interaction then weakening the O-O bonds. Figure 2.18 shows the Tafel plots of Pt and PtFe alloys for the O_2 reduction reaction. The Tafel slopes for the two catalysts are the same. However, the exchange current density of oxygen reduction on PtFe is higher than on Pt. In the Tafel region of 120 mV/dec, the exchange current density for a Pt catalyst is 1.63×10^{-8} A/cm², while that for PtFe catalysts is 2.15×10^{-7} A/cm², indicating a nine-fold increase [47].

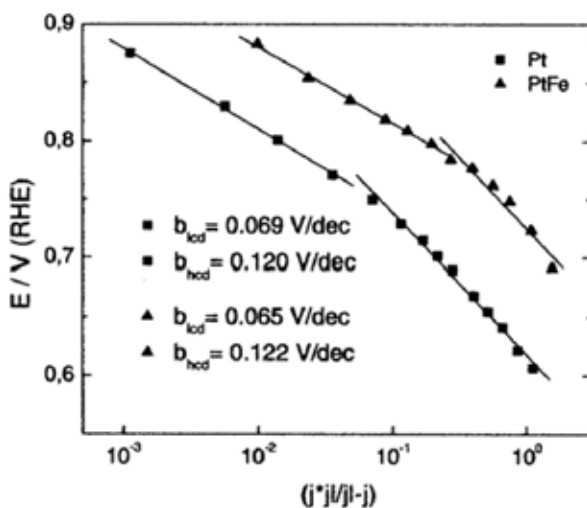


Figure 2.18. Tafel plots for ORR in 0.5 M H_2SO_4 on different catalysts; b_{lod} : Tafel slope at low current density; b_{hcd} : Tafel slope at high current density [47]. (With kind permission from Springer Science+Business Media: Journal of Applied Electrochemistry, Electrocatalytic behaviour for oxygen reduction reaction of small nanostructured crystalline bimetallic Pt-M supported catalysts, 36, 2006, 1143–1149, A. Stassi, Figure 9, ©Springer.)

Stamenkovic et al. [48] recently found that on Pt_3Ni , the O_2 reduction reaction is 90 times faster than on pure Pt. Unfortunately, dissolution of the transition metal alloyed in the PtM catalysts is a major drawback because these transition metals are electrochemically soluble at a potential range between 0.3 to 1 V vs. NHE in low pH media [47]. More effort is needed to solve this problem.

2.4.5 Catalytic ORR on Other Metals

Oxygen reduction reaction on other metal surfaces such as Au, Ir, Rh, etc. has also been extensively investigated [46]. However, these metals show lower catalytic activity towards ORR than Pt; in addition, they are not electrochemically stable (and therefore are more easily oxidized than Pt).

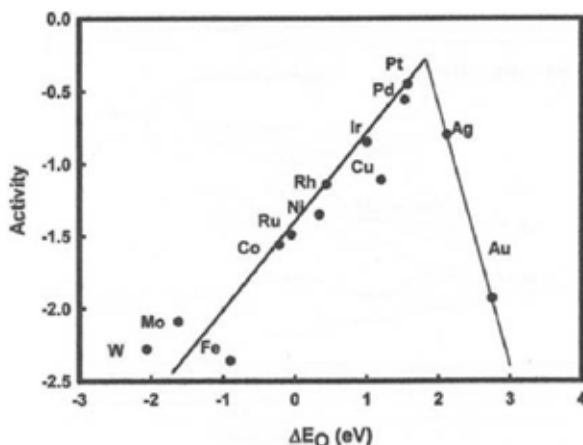


Figure 2.19. Trends in oxygen reduction activity plotted as a function of the oxygen binding energy [44]. (Reprinted with permission from J Phys Chem B 2004;108:17886–92. Copyright 2004 American Chemical Society.)

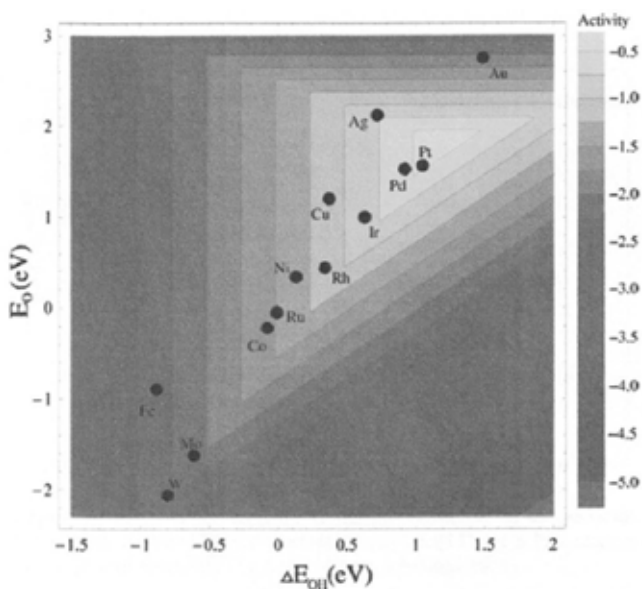


Figure 2.20. Trends in oxygen reduction activity plotted as a function of both the O and the OH binding energy [44]. (Reprinted with permission from J Phys Chem B 2004;108:17886–92. Copyright 2004 American Chemical Society.)

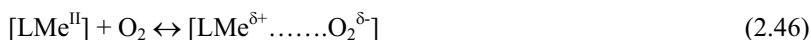
Figure 2.19 shows the trend in oxygen reduction activity as a function of the oxygen binding energy, and Figure 2.20 shows the trend as a function of both the O and the OH binding energy. Both figures show that Pt is the most active ORR catalyst.

2.5 ORR on Macrocyclic Transition Metal Complexes

2.5.1 ORR Mechanisms Catalyzed by Transition Metal Macrocyclic Complexes

Transition metal macrocyclic complexes can catalyze the O₂ reduction reaction through a 2-electron or 4-electron transfer pathway to produce either H₂O₂ or H₂O. Sometimes, they can also catalyze ORR through a mixed pathway of 2- and 4-electron transfer reduction. In rare cases, transition metal macrocyclic complexes can also catalyze a 1-electron O₂ reduction, producing superoxide ions.

The catalytic reaction mechanism is proposed to be a modified “redox catalysis” procedure [1, 49]. In the first step, the adduct between oxygen and the metal ion center of the macrocyclic compound is formed, followed by an intra-adduct electron transfer from the metal ion to the oxygen. The addition of protons from the electrolyte, together with the electron transfer, then produces H₂O₂. The H₂O₂ is either the final product or can be further reduced to produce water, depending on the individual transition metal macrocyclic compounds used. The mechanism can be summarized as follows:



where L represents the ligand and Me is the metal center.

2.5.2 Transition Metal Macrocycles as ORR Catalysts

2.5.2.1 Metal Centers and the Ligand Effect on ORR Activity

The catalytic activity of transition metal macrocyclic compounds towards ORR strongly depends on the individual transition metal center and the macrocyclic ligand, as well as the size of the π electron system. Compounds studied previously include a variety of metal centers and ligands. The transition metals used in macrocyclic catalysts include Fe, Co, Ni, and Cu, and the macrocyclic ligands include chelating atoms N₄, N₂O₂, N₂S₂, O₄, and S₄. The conjugate π electron

compounds usually include metal phthalocyanine and porphyrin, as well as their derivatives [1, 49].

The activity of these compounds changes with respect to the central metal ions in the following order: $\text{Fe} > \text{Co} > \text{Ni} > \text{Cu}$. For a metal center, the chelating atoms of the macrocyclic ring can also change the ORR activity. For example, the active sequence of Fe complexes is as follows: $\text{N}_4 > \text{N}_2\text{O}_2 > \text{N}_2\text{S}_2 > \text{O}_4 \approx \text{S}_4$ (inactive); for Co centers: $\text{N}_2\text{O}_2 > \text{N}_4 > \text{N}_2\text{S}_2 > \text{O}_4 \approx \text{S}_4$; for Cu centers: $\text{N}_4 > \text{O}_4 > \text{N}_2\text{O}_2 > \text{N}_2\text{S}_1 > \text{S}_4$ (inactive); and for Ni centers: $\text{O}_4 > \text{N}_2\text{O}_2 > \text{N}_2\text{S}_2 > \text{N}_4$. With respect to these active sequences, recent research has mainly focused on Fe and Co centers, and for macrocyclic rings, on the N_4 system. In this section, the discussion will focus on the Fe- N_4 and Co- N_4 systems.

2.5.2.2 M- N_4 ORR Catalysts

M- N_4 complexes can strongly and irreversibly adsorb on a graphite electrode surface to form a monolayer or multilayers of ORR catalysts. This adsorption can create a well-defined electrode surface, then provide a theoretical treatable situation for fundamental understanding of the catalyst activity and mechanism [50–52].

For Fe-based N_4 catalysts (Fe- N_4), the ORR normally takes a 4-electron transfer pathway to produce H_2O , as reported by Zagal et al. [50]. Shi et al. [51] found that oxygen reduction catalyzed by Fe tetrakis(4-N-methylpyridyl) porphyrin produced a mixture of H_2O and H_2O_2 . With respect to the ligand effect, Shigehara et al. [52] found that ligands had a strong effect on the ORR activity catalyzed by Fe porphyrins; both Fe meso-tetraphenylporphine (FeTPP) and Fe protoporphyrin IX (FePPiX) can catalyze a 4-electron oxygen reduction, while Fe meso-tetra(3-pyridyl)porphine (FeTPyP) only catalyzes a 2-electron oxygen reduction [51, 52]. Nonetheless, in most cases, Fe- N_4 can catalyze 4-electron oxygen reduction and the product is water.

In general, mononuclear Co- N_4 complexes can only catalyze 2-electron O_2 reduction reaction. Zagal et al. [50] studied Co and Fe tetrasulfonate phthalocyanines and found that the Co complex only catalyzed a 2-electron oxygen reduction process. However, bi-nuclear Co- N_4 complexes or Co- N_4 dimers have some different behaviors from those of mononuclear Co- N_4 complexes. They can catalyze not only 2-electron but also 4-electron O_2 reduction reactions. A planar bi-cobalt complex such as $(\text{Co}_2\text{TAPH})^{4+}$, as shown in Figure 2.21, catalyzes a 4-electron reduction of O_2 in alkaline solutions. This catalytic activity was found to be due to the interaction between O_2 and the Co metal centers. This interaction can effectively weaken the O-O bond, rendering it easily broken. Furthermore, face-to-face di-Co- N_4 complexes also favor a 4-electron transfer pathway, depending on the Co-Co distance in the molecules (Figure 2.22). When the Co-Co distance is around 4 Å, the O-O bridge between the Co-Co centers can be formed as shown in Figure 2.23, resulting in a 4-electron transfer of ORR. If the Co-Co distance is larger or smaller, only the 2-electron transfer pathway to peroxide is favored. This can be explained by the formation of a cis- or trans-configuration (Figure 2.23). The cis-configuration favors the 4-electron ORR to H_2O , while the trans- does not [53].

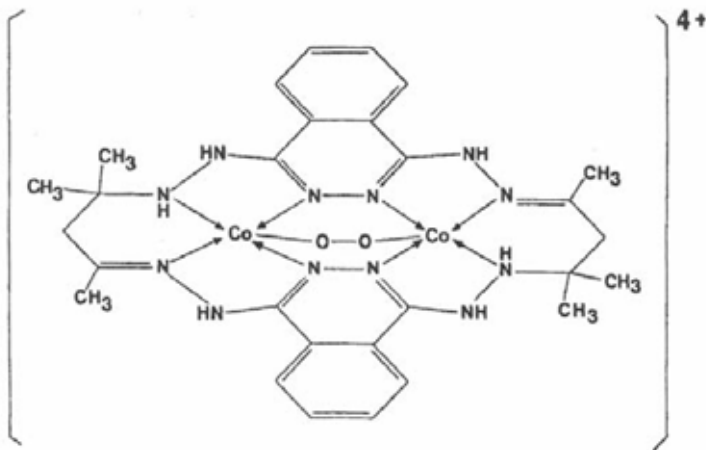


Figure 2.21. Dimetal complex $(\text{Co}_2\text{TAPH})^{4+}(\text{NO}_3)_4$. (TAPH = 6,7,8,9,12,19, 20,21,22,25-decahydro-8,8,10,21,21,23,-hexamethyl-5,26:13,18-bis(azo)-dibez(1,2,6,7,12,13,17,18)oxa-azacyclodocosine) [2]. (Reprinted from Journal of Molecular Catalysis, 38(1–2), Yeager Ernest, Dioxygen electrocatalysis: mechanisms in relation to catalyst structure, 5–25, ©1986, with permission from Elsevier.)

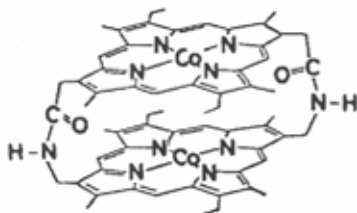


Figure 2.22. Face-to-face Co-Co 4-porphyrin [2]. (Reprinted from Journal of Molecular Catalysis, 38(1–2), Yeager Ernest, Dioxygen electrocatalysis: mechanisms in relation to catalyst structure, 5–25, ©1986, with permission from Elsevier.)

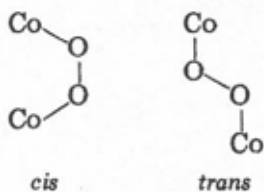


Figure 2.23. Cis- and trans-Co-O-O-Co facial configuration [2]. (Reprinted from Journal of Molecular Catalysis, 38(1–2), Yeager Ernest, Dioxygen electrocatalysis: mechanisms in relation to catalyst structure, 5–25, ©1986, with permission from Elsevier.)

Recently, Kadish et al. [54] synthesized three series of Co corroles (shown in Figure 2.24) and investigated their catalytic activity toward the O_2 reduction reaction [54]. The mixed valent Co(II)/Co(III) complexes, $(\text{PCY})\text{Co}_2$, and the

biscorrole complexes, (BCY)Co₂, both contain two Co(III) ions in their air-stable forms. It was found that all of these complexes could catalyze the direct 4-electron pathway for O₂ reduction to H₂O in aqueous acidic electrolyte. The most efficient catalysis process was observed when the complex had an anthracene spacer. This catalyzed 4-electron transfer pathway was further confirmed by RRDE measurement. Only a relatively small amount of hydrogen peroxide was detected at the ring electrode in the vicinity of $E_{1/2}$: 0.47 V vs. SCE for (PCA)Co₂ and 0.39 V for (BCA)Co₂, respectively. The cobalt(III) monocorrole (Me₄Ph₅Cor)Co could also catalyze ORR at $E_{1/2}$ = 0.38 V, with the final products being an approximate 50% mixture of H₂O₂ and H₂O.

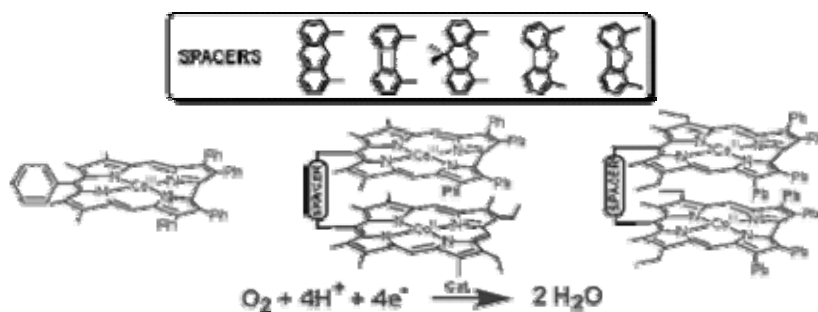


Figure 2.24. Co-corrole compounds for O₂ reduction reaction [54]. (Reprinted with permission from J Am Chem Soc 2005;127:5625–31. Copyright 2005 American Chemical Society.)

Theoretical approaches have in addition predicted that the substituents on the macrocyclic rings can also affect ORR catalytic activity. Co-phthalocyanine complexes with electron donating substituents should show improved ORR catalytic activity because the substituents can increase the binding energy between O₂ and the metal center(s) [55]. Calculation indicates that the catalytic activity of the transition metal macrocyclic complexes is due to the partial electron transition between the filled d_{xz} , d_{yz} , and empty d_{z^2} orbitals of the transition metals, and the anti-bonding π orbitals of O₂. Based on molecular orbital theory, Alt et al. [56] explained that in the interaction between O₂ and a transition metal, electron transition occurs first from oxygen into the empty d_{z^2} orbital, forming a σ bond, lowering the anti-bonding π orbitals and raising the energy of the d_{xz} and d_{yz} orbitals of the transition metals, thus allowing the electron transition from these filled orbitals to the anti-bonding π orbital, and resulting in enhanced interaction. The order of catalytic ORR activity for both the tetramethoxyphenylporphyrin (TMPP) and the dihydrodibenzotetraazaannulene (DHDBTAA) systems is: Co > Fe > Ni \approx Cu. This order can be well explained in terms of molecular orbital theory [49, 56].

2.5.2.3 Heat-treated Transition Metal Macrocyclic Complexes

Normally, transition metal macrocyclic complexes do not have long-term stability in concentrated acidic or alkaline solutions. It has been found that thermal

treatment of these compounds after they have been adsorbed on high-surface-area carbon support particles in the temperature range of 450–900 °C not only increases their stability, but also improves their catalytic activity [1, 2, 57]. The thermal treatment was performed in an inert atmosphere, where pyrolysis of the compounds would occur. Thermal treatment temperature can affect the stability and catalytic activity of the M-N₄ compounds, and usually high temperature (> 800 °C) is necessary to obtain stable catalysts.

Although heat treatment can destroy the macrocyclic ring, the N₄ ring structure in porphyrin and similar macrocycles is still retained. Heat treatment can also be performed by heat-treating the macrocycles adsorbed on carbon substrates, followed by the addition of transition metal salts. The pyrolyzed macrocycles on carbon supports provide coordination sites, including N₄, to bind transition metals such as Fe and Co, forming M-N₄ coordination complexes. However, it was also found that the ORR catalytic activity loss of these heat-treated M-N₄ catalysts in long-term operation was due to the loss of the transition metal from the pyrolyzed macrocycle surface.

Thermal treatment might lead to phase change in the transition metal macrocyclic complexes. Using XRD measurements, Baranton [58] found that received iron phthalocyanine was under α phase and that after being heat-treated at 450 °C it was under β phase.

It is worth noting that as yet, the enhancement mechanisms of activity and stability after heat treatment of these M-N₄ catalysts are not fully understood. It is necessary to ascertain whether the metal is part of the active catalytic site, and also to identify the nature of the catalytic site.

2.5.3 ORR Kinetics Catalyzed by Transition Metal Macrocyclic Complexes

Tafel slopes of ORR catalyzed by M-N₄ complexes have different values, depending on the individual catalyst used. Zagal et al. [50, 59] reported that Co(II) tetrasulfonatephthalocyanine (CoTSP) could catalyze a 2-electron O₂ reduction reaction, producing H₂O₂ in both acid and alkaline solutions, with Tafel slope values of 120, 135, and 155 mV/dec, respectively. Collman et al. [60] reported a Tafel slope of 65 mV/dec on dicobalt porphyrin dimers in acid solution. For Fe-N₄ catalysts, Zagal et al. [50] reported two Tafel slopes of FeTSP catalyzed oxygen reduction reaction, which were dependent on pH. At low overpotential, a Tafel slope of 65 mV/dec was obtained at pH 4.4, which decreased to 29 mV/dec when pH was increased to 13.9. At high overpotential, a Tafel slope of 120 mV/dec was observed at pH 4.4, which changed slightly to 130 mV/dec at pH 13.8. These two Tafel slopes are the same as those reported by Baranton et al. [58] for α -FePc-catalyzed ORR in acid solution. However, for β -FePc, only one Tafel slope (63 mV/dec) was obtained, indicating that the ORR mechanism was different.

The exchange current density of ORR catalyzed by M-N₄ complexes is seldom reported. Zagal et al. [59] found that in acid solution, ORR catalyzed by Co(II)TSP had an exchange current density of 10⁻¹¹ A/cm² for O₂/H₂O reaction, while in alkaline solution, the value became 10⁻⁷ A/cm². Note that in both solutions, Co(II)TSP could only catalyze a 2-electron O₂ reduction reaction. In the early stage of M-N₄-catalyzed ORR research, Savy et al. [61] studied ORR catalyzed by

porphyrin complexes with Fe, Co, Ni, and Cu metal centers, and they reported the exchange current densities of ORR catalyzed by each. For example, FePc showed exchange current densities of 1.3×10^{-7} A/cm² at pH 1.3 and 1.5×10^{-8} A/cm² at pH 6.7.

2.6 ORR Catalyzed by Other Catalysts

2.6.1 ORR Catalyzed by Transition Metal Chalcogenides

2.6.1.1 Chalcogenides and Oxygen Reduction Reaction Products

Transition metal chalcogenides are a group of materials that show catalytic activity towards ORR. The materials are classified into two types, based on the structure, the Chevrel phase-type compounds such as Mo₄Ru₂Se₈, and amorphous phase compounds such as Ru_xS_y [1]. Figure 2.25 shows the structure of Mo₄Ru₂Se₈, where the octahedral transition metal core acts as an electron reservoir [62].

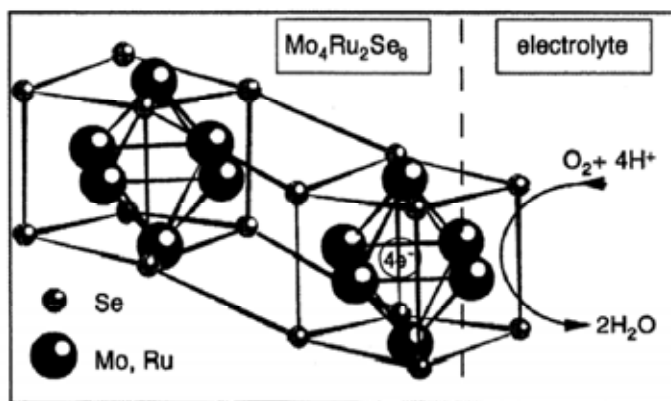


Figure 2.25. Structure of Mo₄Ru₂Se₈ and interaction of O₂ at the Chevrel phase clusters-electrolyte interface [62]. (Reprinted from J Phys IV, Alonso-Vante N, Fieber-Erdmann M, Rossner H, Holub-Krappe E, Giorgetti Ch, Tadjeddine A, et al. The catalytic center of transition metal chalcogenides vis-à-vis the oxygen reduction reaction: an *in situ* electrochemical EXAFS study, 7:887–9. ©1997 with permission of EDP Sciences.)

Chalcogenides can catalyze either 2-electron or 4-electron O₂ reduction, depending on the catalysts used. For example, Mo₄Ru₂Se₈, Ru_{1.92}Mo_{0.08}SeO₄, Ru_xS_y(CO)_n, Ru_xSe_y, etc. catalyze 4-electron transfer [62–68], while W-Co-Se catalyzes a 2-electron O₂ reduction reaction [69].

2.6.1.2 Chalcogenide-catalyzed ORR Mechanism

The origin of the ORR catalytic activity of a chalcogenide is strongly associated with its semiconducting property. It is believed that the catalytic activity occurs through the interaction of O₂ with the transition metal d-states originating from the mixed metal cluster. Figure 2.26 shows the schematic of the energy and molecular

statuses of the semiconducting cluster at the interface, under charge transfer conditions.

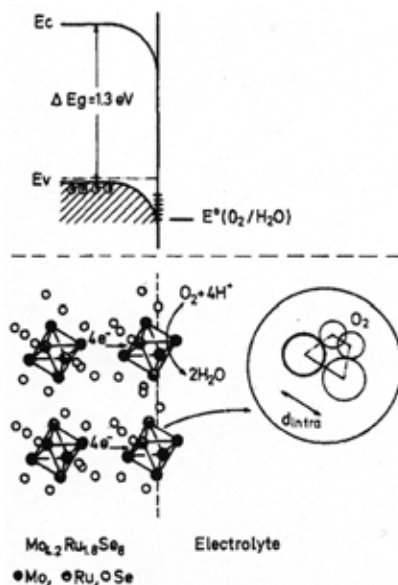


Figure 2.26. Schematic energy and molecular representation of the semiconducting $\text{Mo}_{4.2}\text{Ru}_{1.8}\text{Se}_8$ cluster and the redox couple ($\text{O}_2/\text{H}_2\text{O}$) at the interface, under charge transfer conditions. The insert shows a supposed interaction of the molecular bridge type at two adjacent transition metal atoms [63]. (Reprinted with permission from J Am Chem Soc 1987;109:3251–7. Copyright 1987 American Chemical Society.)

In this $\text{Mo}_{4.2}\text{Ru}_{1.8}\text{Se}_8$ compound, the energy gap between the valence and the conductance band is 1.3 eV, which is a characteristic of the compound as a degenerated p-type semiconductor. The O_2 reduction reaction will start when the Fermi level of the electrode is 0.35 V above the $\text{O}_2/\text{H}_2\text{O}$ redox potential. It is most possible that O_2 interacts with a transition metal atom of a cluster through a bridge-type bonding to two adjacent metal atoms in the same cluster. The electron transfer between the cluster and the O_2 could result in a metal distance increase, which possibly facilitates the breaking of the O-O bond and an upward shift of the electronic level due to the loss of electrons. The cluster volume can increase by 15% when it loses its electrons. Refilling of the cluster with electrons is expected because the Fermi level is above the edge of the valence band [63].

The ORR mechanism catalyzed by a chalcogenide is different from that catalyzed by Pt or other catalysts. Although the mechanism is still not clear, most possibly it is not a stepwise subsequent electron process involving an intermediate. Rather, it may involve a synergistic multielectron transfer, or a self-organized electron transfer. The electrons are not transferred independently, but rather are dependent on each other. An initiating electron transfer event could produce a “positive friction” loop, triggering subsequent loops. If the feedback can be adjusted adequately, the electrons will transfer in a cooperative way without producing

intermediates [70, 71]. This feedback is possibly reflected in the distance change between the metal atoms.

2.6.1.3 Kinetics of ORR Catalyzed by Chalcogenides

The catalytic activity of a chalcogenide towards ORR can reach a level of 30–40% of the Pt catalyst activity. The Tafel slope varies from 100 mV/dec up to 167 mV/dec, depending on the materials used and the preparation method. Duron et al. [66] reported two Tafel slopes for ORR on a $\text{Ru}_x\text{S}_y(\text{CO})_n$ cluster: 124 mV/dec at low overpotential and 254 mV/dec at high overpotential. Susac et al. [72] reported a Tafel slope of 167 mV/dec on Co-Se catalyst. There seems to be no reported data in the literature about the exchange current density of ORR catalyzed by chalcogenides.

2.6.2 ORR Catalyzed by Transition Metal Carbide

Transition metal carbide, in particular tungsten carbide, is another type of non-noble catalyst showing activity towards the oxygen reduction reaction. However, the main catalytic activity of carbide is not in the oxygen reduction reaction, but rather in other reactions such as H_2 oxidation. Mazza et al. [73] reported that WC, TaC, TiC, and TiN showed catalytic activity towards ORR in acid solutions. However, these materials are not stable in alkaline solution. For example, even in acid solutions, WC did not show long-term stability in the presence of O_2 [73]. Lee et al. [74] found that the addition of Ta to WC could significantly improve its catalytic activity and stability.

Although pure WC has no significant ORR catalytic activity, the addition of it to Pt could lead to an improvement [75, 76]. Figure 2.27 shows the linear sweep curves of ORR on W_2C , Pt/C, and W_2C -Pt/C catalysts. The best activity can be observed with a W_2C -Pt/C catalyst.

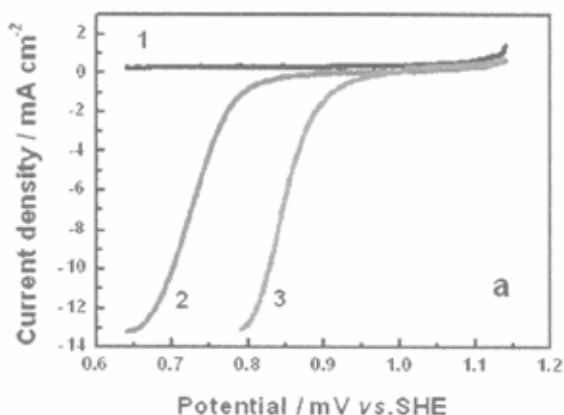


Figure 2.27. Linear sweep curves of oxygen reduction on different catalysts in O_2 -saturated 0.5 M H_2SO_4 solution at 25 °C: curve 1, 80 μg W_2C ; curve 2, 80 μg Pt/C; curve 3, 40 μg Pt+80 μg W_2C ; scan rate: 2 mV/s [75]. (Reprinted with permission from J Phys Chem B 2005;109:22705–9. Copyright 2005 American Chemical Society.)

The mechanism of the ORR activity enhancement induced by adding W_2C to Pt is not yet clear. Experimental results show that most possibly this is due to the synergistic effect between tungsten carbide nanoparticles and Pt at the interface.

There seems to be no report about the Tafel slope of WC-catalyzed ORR. The Tafel slope of W_2C -Pt/C-catalyzed ORR is similar to that of Pt/C: 66 mV/dec at low overpotential and 126 mV/dec at high overpotential. The presence of W_2C can significantly decrease ORR overpotential, as shown in Figure 2.28.

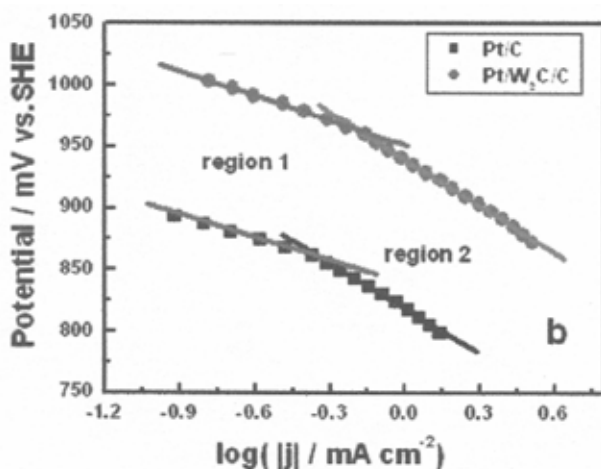


Figure 2.28. Tafel slopes for oxygen reduction reaction on Pt/C and Pt- W_2C /C electrocatalysts [75]. (Reprinted with permission from J Phys Chem B 2005;109:22705–9. Copyright 2005 American Chemical Society.)

The exchange current density of ORR on W_2C -Pt/C could also be increased. For example, Pt/C gave two exchange current densities: 5.25×10^{-10} A/cm² at low overpotential and 3.16×10^{-7} A/cm² at high overpotential. While on W_2C -Pt/C, the values were found to be 4.7×10^{-7} A/cm² at low overpotential and 5.01×10^{-5} A/cm² at high overpotential, showing a two- to three-order increase compared to pure Pt/C catalyst [75].

2.7 Superoxide Ion

2.7.1 Production of Superoxide Ion by Other Methods

Superoxide ion is an important intermediate in the fundamental understanding of the ORR mechanism. This species has significant implications in chemistry and biology. Superoxide ion was initially produced from radiolysis. In a solution containing a large excess of sodium formate saturated with O_2 , the radiolytic electron flux could reduce O_2 to produce O_2^- [77,78]:





Superoxide ion could be also produced by an electrochemical method in aprotic organic solvents [79–83], in ionic liquid systems (room temperature) [84–87], on organic-compound-coated electrode surfaces [88], and on Co-macrocyclic-complex-coated electrodes [89, 90]. The electrochemical response of superoxide ion is reversible in aprotic organic solvents such as DMSO, and in ionic liquid systems.

2.7.2 Properties of Superoxide Ion

The thermodynamic reduction potential for the O_2/O_2^- pair has been determined using redox mediator dyes and spectrophotometry [77, 78]. The reaction is expressed as: $\text{O}_2(\text{g}, 1 \text{ atm}) + \text{e}^- \leftrightarrow \text{O}_2^-$, and its corresponding standard electrode potential is $(E^0)_{\text{pH},5-14} = -0.33 \text{ V vs. NHE}$ or -0.16 V for O_2 at unit activity. The redox potential of the O_2/O_2^- is dependent on the solvent and the electrode materials. Table 2.4 summarizes the redox potentials of O_2/O_2^- , concentration and the diffusion coefficient of O_2 in different solvents. The formal potential was taken as the average of the anodic peak and the cathodic peak potentials from CV at a scan rate of 0.1 V/s .

Table 2.4. Redox potentials for O_2/O_2^- in different solvents (1 atm O_2) [78–86]

Solvent	C_{O_2} (mM)	$\text{D}_{\text{O}_2} \times 10^5$ ($\text{cm}^2 \text{ s}^{-1}$)	E^0 (V) vs. NHE
H_2O	1.0	2.1	−0.16
DMSO	2.1	2.1	−0.54
DMF	4.8	5.0	−0.62
Py	4.9	5.7	−0.62
MeCN	8.1	7.2	−0.63
Quinoline	1.5	1.8	−0.63
EMIBF ₄	1.1	1.7	−0.61
PMIBF ₄	1.0	1.3	−0.58
BMIBF ₄	1.1	1.2	−0.62
[bmim]HFP	3.6	0.22	−0.64
Hydrocarbons	~10	-	-
Fluorocarbons	~25	-	-

Table 2.5. The formal potentials at different electrode materials [78]

Solvent	Formal potentials at electrodes (V) vs. NHE			
	C	Pt	Au	Hg
DMSO	−0.54	−0.78	−0.55	-
DMF	−0.62	−0.62	−0.64	-
Py	−0.64	−0.65	−0.63	
MeCN	−0.63	−0.65	−0.65	−0.63

The formal potential change with solvent is due to the salvation energy of O_2^- in different solvents. The value becomes more positive with increasing salvation energy. Thus, the salvation energy of O_2^- in these aprotic solvents follows the sequence:



2.7.3 Stability of Superoxide Ion

Superoxide ion is not stable in the presence of water and protonic species, which results in the disproportionation of the superoxide ions and leads to the production of H_2O_2 [78, 79, 84], according to Equation 2.55:

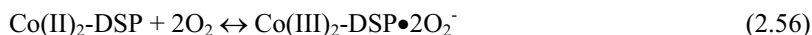


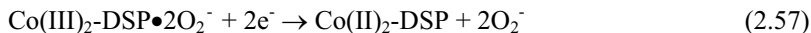
2.7.4 Superoxide Production by Electrocatalysis

In aqueous systems, superoxide ion was only observed on electrodes modified in alkaline solutions by surfactant (triphenylphosphine oxide) [91], organic groups (methyl phenyl) [88], or metal macrocyclic compounds [88, 89, 92]. The surfactant and organic groups can cover the electrode surface, preventing water from reaching the electrode surface and stabilizing the produced O_2^- . The reversibility of the O_2/O_2^- electrochemical response depends on the alkalinity [88, 90]. In less alkaline solutions, the redox behavior becomes less reversible, due to the kinetics of the reaction.

Superoxide ion production by electrocatalysis was observed on Fe(III) phthalocyanine, Co(II)₂-disalophen, and Co(II)HFPC-modified Hg or carbon electrodes. However, on Fe(III)phthalocyanine-modified Hg electrode surfaces, further scanning the potential to more negative values resulted in further reduction of O_2^- , forming H_2O_2 and OH^- [92]. On Co(II)₂-DSP and Co(II)HFPC modified electrodes [89, 90], stable superoxide ion could be produced in alkaline solutions. The catalytic mechanism has been proposed as follows:

For Co(II)₂-DSP:





For Co(II)HFPC:

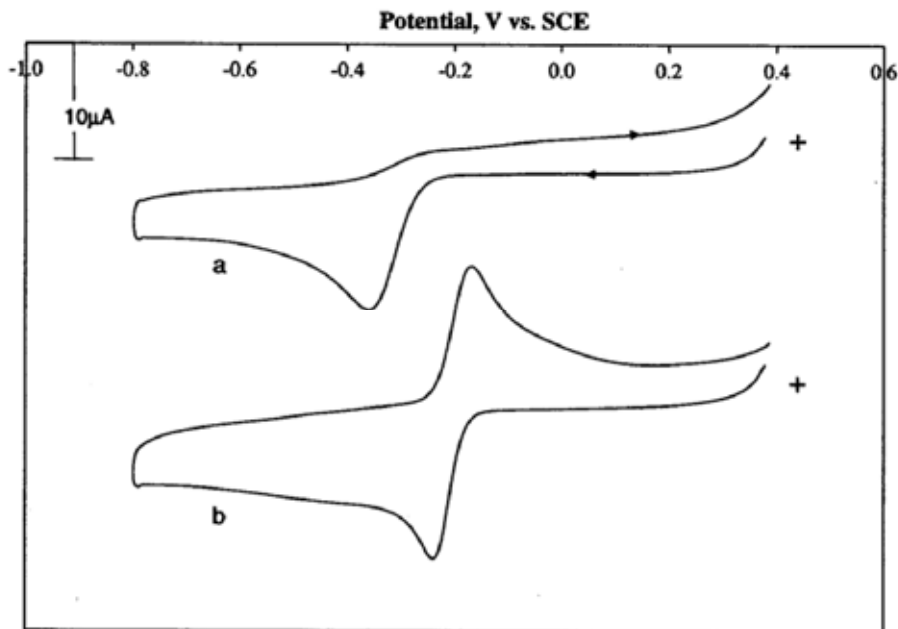
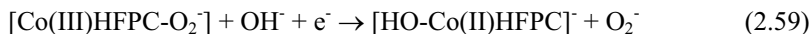
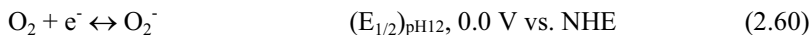


Figure 2.29. (a) Cyclic voltammograms of a bare graphite electrode and (b) a Co^{II}HFPC adsorbed graphite electrode in an air-saturated 1 M NaOH solution. Scan rate: 50 mV/s [90]. (Reprinted from Journal of Electroanalytical Chemistry, 587(2), Song C, Zhang L, Zhang J, Reversible one-electron electro-reduction of O₂ to produce a stable superoxide catalyzed by adsorbed Co(II) hexadecafluoro-phthalocyanine in aqueous alkaline solution, 293–8, ©2006, with permission from Elsevier.)

The formal potential of the O₂/O₂⁻ redox couple is very close to the redox potential of the catalyst. For both Co(III)₂-DSP and Co(II)HFPC systems, the formal potential of O₂/O₂⁻ is ~0.0 V vs. NHE, normalizing the air pressure to O₂ pressure. This value is close to that reported in [78] for the initial reversible 1-electron transfer process of O₂ in aqueous solution at inert electrodes:



2.8 Conclusions

The catalytic mechanism of ORR and its kinetic parameters, including Tafel slopes and exchange current densities, can be obtained from techniques such as cyclic voltammetry, steady-state polarization, rotating disk electrode, and rotating ring-disk electrode. Catalysts used for ORR include carbon materials, quinone and derivatives, noble metal and noble metal alloy materials, transition metal macrocyclic compounds, chalcogenide materials, as well as transition metal carbide. Electrocatalytic ORR has been investigated in a wide range of electrolytes, ranging from acid to basic solutions, and in a wide range of solvent systems, including aqueous, non-aqueous aprotic, and room temperature ionic liquid systems.

Electrocatalytic ORR carries out in three pathways: the 1-electron transfer pathway, producing superoxide ion; the 2-electron transfer pathway, producing hydrogen peroxide; and the 4-electron transfer pathway, producing water. In a non-aqueous aprotic solvent system, a room-temperature ionic liquid system, and on specific transition-metal, macrocyclic-compounds-coated graphite electrodes in alkaline solutions, 1-electron reduction can be observed. Carbon materials, quinone and derivatives, mono-nuclear cobalt macrocyclic compounds, and some chalcogenides can only catalyze 2-electron ORR. Noble metal, noble metal alloy materials, iron-macrocyclic complexes, di-nuclear cobalt macrocyclic complexes, some chalcogenides, and transition-metal carbide-promoted Pt catalysts can catalyze 4-electron reduction.

The Tafel slope of the electrocatalytic ORR is usually 60 mV/dec or 120 mV/dec, or both 60 and 120 mV/dec, depending on the overpotential range. On carbon materials, a Tafel slope of either 60 or 120 mV/dec was observed depending on the pH of the electrolyte and on the carbon materials. On noble metal and noble metal alloys, two Tafel slopes were observed at different overpotential regions. At low overpotential (low current density), a Tafel slope of 60 mV/dec was obtained, while at high overpotential (high current density), a Tafel slope of 120 mV/dec was observed. On chalcogenide catalysts, Tafel slopes of larger than 120 mV/dec were reported. On other materials, Tafel slopes have rarely been studied.

The exchange current density of electrocatalytic ORR is mainly reported on Pt and Pt alloy catalysts. Because there are two Tafel regions, two exchange current densities can be obtained. At low overpotential, the exchange current density is around 10^{-10} A/cm², and at high overpotential, the exchange current density is around 10^{-6} A/cm². The values of exchange current density vary depending on the catalyst as well as the research method. On other catalysts, the exchange current density of ORR has seldom been reported.

References

1. Zhang L, Zhang J, Wilkinson DP, Wang H. Progress in preparation of non-noble electrocatalysts for PEM fuel cell reactions. *J Power Sources* 2006;156.2:171–82.

2. Yeager E. Dioxygen electrocatalysis: mechanism in relation to catalyst structure. *J Mol Catal* 1986;38:5–25.
3. Bard AJ, Faulkner LR. *Electrochemical methods: fundamentals and applications*. New York: Wiley, 1980.
4. Song C, Tang Y, Zhang J, Zhang J, Wang H, Shen J, et al., PEM fuel cell reaction kinetics in the temperature range of 23–120 °C. *Electrochim Acta* 2007;52:2552–61.
5. Damjanovic A. Temperature dependence of symmetry factors and the significance of the experimental activation energies. *J Electroanal Chem* 1993;355:57–77.
6. Zhang J, Tang Y, Song C, Xia Z, Wang H, Zhang J, et al. Effect of relative humidity on PEM fuel cell performance at elevated temperature. *Forthcoming* 2008.
7. Parthasarathy A, Srinivasan S, Appleby AJ, Martin CR. Temperature dependence of the electrode kinetics of oxygen reduction at the platinum/Nafion interface – a microelectrode investigation. *J Electrochem Soc* 192;139:2530–7.
8. Wkabayashi N, Takeichi M, Itagaki M, Uchida H, Watanabe M. Temperature dependence of oxygen reduction activity at a platinum electrode in an acidic electrolyte solution investigated with a channel flow double electrode. *J Electroanal Chem* 2005;574:339–46.
9. Baker R, Wilkinson DP, Zhang J. Electrocatalytic activity and stability of substituted iron phthalocyanines towards oxygen reduction evaluated at different temperatures. *Electrochim Acta*. *Forthcoming* 2008.
10. Lever ABP. The phthalocyaninids-molecules of enduring value: a two-dimensional analysis of redox potentials. *J Porphyrins Phthalocyanines* 1999;3:488–99.
11. Zhang L, Song C, Zhang J, Wang H, Wilkinson DP. Temperature and pH dependent oxygen reduction catalyzed by iron fluoro-porphyrin adsorbed on a graphite electrode. *J Electrochem Soc* 2005;152:A2421–6.
12. Song C, Zhang L, Zhang J, Wilkinson DP, Baker R. Temperature dependence of oxygen reduction catalyzed by cobalt fluorophthalocyanine adsorbed on a graphite electrode. *Fuel Cells* 2007;7:9–15.
13. Antoine O, Durand R. RRDE study of oxygen reduction on Pt nanoparticles inside Nafion: H₂O₂ production in PEMFC cathode conditions. *J Appl Electrochem* 2000;30:839–844.
14. Taylor RJ, Humffray AA. Electrochemical studies on glassy carbon electrodes II. Oxygen reduction in solutions of high pH (pH>10). *J Electroanal Chem* 1975;64:63–84.
15. Paliteiro C, Hamnett A, Goodenough JB. The electroreduction of oxygen on pyrolytic graphite. *J Electroanal Chem* 1987;233:147–59.
16. Zhang M, Yan Y, Gong K, Mao L, Guo Z, Chen Y. Electrostatic layer by layer assembled carbon nanotube multilayer film and its catalytic activity for oxygen reduction reaction. *Langmuir* 2004;20:8781–5.
17. Taylor RJ, Humffray AA. Electrochemical studies on glassy carbon electrodes II. Oxygen reduction in solutions of low pH (pH<10). *J Electroanal Chem* 1975;64:85–94.
18. Davis M, Clark M, Yeager E, Hovorka F. Oxygen electrode. *J Electrochem Soc* 1959;106:56.
19. Appel M, Appleby AJ. A ring disk electrode study of the reduction of oxygen on active carbon in alkaline solution. *Electrochim Acta* 1978;23:1243–6.
20. Jurmann G, Tammeveski K. Electroreduction of oxygen on multi-walled carbon nanotube modified highly oriented pyrolytic graphite electrodes in alkaline solution. *J Electroanal Chem* 2006;597:119–26.
21. Baez VB, Pletcher D. Preparation and characterization of carbon/titanium dioxide surfaces – the reduction of oxygen. *J Electroanal Chem* 1995;382:59–64.
22. Morcos I, Yeager E. Kinetic studies of the oxygen-peroxide couple on pyrolytic graphite *Electrochim Acta* 1970;15:953–75.

23. Maldonado S, Stevenson KJ. Influence of nitrogen doping on oxygen reduction electrocatalysis at carbon nanofiber electrodes. *J Phys Chem B* 2005;109.10:4707–16.
24. Sidik RA, Anderson AB, Subramanian NP, Kumaraguru SP, Popov BN. O₂ reduction on graphite and nitrogen doped graphite: experiment and theory. *J Phys Chem B* 2006;110:1787–93.
25. Hu I, Karweik DH, Kuwana T. Activation and deactivation of glassy carbon electrodes. *J Electroanal Chem* 1985;188:59–72.
26. Sljukic B, Banks CE, Compton RG. An overview of the electrochemical reduction of oxygen at carbon based modified electrodes. *J Iranian Chem Soc* 2005;2:1–25.
27. Maruyama J, Abe I. Cathodic oxygen reduction at the interface between Nafion and electrochemically oxidized glassy carbon surfaces. *J Electroanal Chem* 2002;527:65–70.
28. Jia N, Martin RB, Qi Z, Lefebvre MC, Pickup PG. Modification of carbon supported catalysts to improve performance in gas diffusion electrodes. *Electrochim Acta* 2001;46:2863–9.
29. Sullivan MG, Kotz R, Haas O. Thick active layers of electrochemically modified glassy carbon, electrochemical impedance studies. *J Electrochem Soc* 2000;147:308–17.
30. Huissoud A, Tissot P. Electrochemical reduction of 2-ethyl-9,10-anthraquinone (EAQ) and mediated formation of hydrogen peroxide in a two-phase medium. *J Appl Electrochem* 1999;29:11–25.
31. Chen Q. Toward cleaner production of hydrogen peroxide in China. *J Cleaner Production* 2006;14:708–12.
32. Huissoud A, Tissot P. Electrochemical reduction of 2-ethyl-9,10-anthraquinone on reticulated vitreous carbon and mediated formation of hydrogen peroxide. *J Appl Electrochem* 1998;28:653–7.
33. Gyenge EL, Coloman CW. Electrosynthesis of hydrogen peroxide in acidic solutions by mediated oxygen reduction in a three-phase (aqueous/organic/gaseous) system. *J Appl Electrochem* 2003;33:655–63, 665–74.
34. Tammeveski K, Kontturi K, Nichols RJ, Potter RJ, Schiffrin DJ. Surface redox catalysis for O₂ reduction on quinone modified glassy electrodes. *J Electroanal Chem* 2001;515:101–12.
35. Sarapuu A, Helstein K, Schiffrin DJ, Tammeveski K. Kinetics of oxygen reduction on quinone modified HOPG and BDD electrodes in alkaline solution. *Electrochem Solid-State Lett* 2005;8:E30–3.
36. Mirkhalaf F, Tammeveski K, Schiffrin DJ. Substituent effects on the electrocatalytic reduction of oxygen on quinone modified glassy carbon electrodes. *Phys Chem Chem Phys* 2004;6:1321–7.
37. Vaik K, Sarapuu A, Tammeveski K, Mirkhalaf F, Schiffrin DJ. Oxygen reduction on phenanthrenequinone-modified glassy carbon electrodes in 0.1 M KOH. *J Electroanal Chem* 2004;564:159–66.
38. Sarapuu A, Vaik K, Schiffrin DJ, Tammeveski K. Electrochemical reduction of oxygen on anthraquinone modified glassy carbon electrodes in alkaline solution. *J Electroanal Chem* 2003;541:23–9.
39. Keita B, Nadjio L. Catalytic synthesis of hydrogen peroxide: an attractive electrochemical and photoelectrochemical route to the reduction of oxygen. *J Electroanal Chem* 1983;145:431–7.
40. Salimi A, Eshghi H, Sharghi H, Golabi SM, Shamsipur M. Electrocatalytic reduction of dioxygen at the surface of glassy carbon electrodes modified by some anthraquinone substituted podands. *Electroanalysis* 1999;11:114–9.

41. Wilson T, Zhang J, Oloman CC, Wayner DDM. Anthraquinone-2-carboxylic-allyl ester as a new electrocatalyst for dioxygen reduction to produce H_2O_2 . *Int J Electrochem Sci* 2006;1:99–109.
42. Markovic NM, Ross PN. Surface science studies of model fuel cell electrocatalysts. *Surf Sci Rep* 2002;45:117–229.
43. Zhdanov VP, Kasemo B. Kinetics of electrochemical O_2 reduction on Pt. *Electrochem Commun* 2006;8:1132–6.
44. Norskov JK, Rossmeisl J, Logadotir A, Lindqvist L, Kitchin JR, Bligaard T, et al. Origin of the overpotential for oxygen reduction at a fuel cell cathode. *J Phys Chem B* 2004;108:17886–92.
45. Shi Z, Zhang J, Liu Z, Wang H, Wilkinson DP. Current status of ab initio quantum chemistry study for oxygen electroreduction on fuel cell catalysts *Electrochim Acta* 2006;51:1905–16.
46. Hoare JP. The electrochemistry of oxygen. New York: Wiley, 1968.
47. Stassi A, D'Urso C, Baglio V, Di Blasi A, Antonucci V, Arico AS, et al. Electrocatalytic behaviour for oxygen reduction reaction of small nanostructured crystalline bimetallic Pt-M supported catalysts. *J Appl Electrochem* 2006;36:1143–9.
48. Stamenkovic VR, Mun BS, Wang G, Ross PN, Lucas CA, Markovic NM. Improved oxygen reduction activity on $\text{Pt}_3\text{Ni}(111)$ via increased surface site activity. *Science* 2007;315:493–7.
49. Jahnke H, Schonborn M, Zimmermann G. Organic dyestuffs as catalysts for fuel cells. *Top Cur Chem* 1976;61:133–81.
50. Zagal J, Bindra P, Yeager E. A mechanistic study of O_2 reduction on water soluble phthalocyanines adsorbed on graphite electrodes. *J Electrochem Soc* 1980;127:1506–17.
51. Shi C, Anson FC. Catalytic pathways for the electroreduction of O_2 by iron terakis(4-N-methylpyridyl)porphyrin or iron tetraphenylporphyrin adsorbed on edge plane pyrolytic graphite electrodes. *Inorg Chem* 1990;4298–305.
52. Shigehara K, Anson FC. Electrocatalytic activity of three iron porphyrins in the reductions of dioxygen and hydrogen peroxide at graphite electrodes. *J Phys Chem* 1982;86:2776–83.
53. Liu H, Weaver M, Wang C, Chang C. Dependence of electrocatalysis for dioxygen reduction by adsorbed cofacial dicobalt porphyrins upon catalyst structure. *J Electroanal Chem* 1983;145:439–47.
54. Kadish KM, Fremont L, Ou Z, Shao J, Shi C, Anson FC, et al. Cobalt(III) corroles as electrocatalysts for the reduction of dioxygen: reactivity of a monocorrole, biscalcorole, and porphyrin-corrole dyads. *J Am Chem Soc* 2005;127:5625–31.
55. Shi Z, Zhang J. Density functional theory study of transitional metal macrocyclic complexes' dioxygen-binding abilities and their catalytic activities toward oxygen reduction reaction. *J Phys Chem C* 2007;111:7084–90.
56. Alt H, Binder H, Sandstedt G. Mechanism of electrocatalytic oxygen reduction on metal chelates. *J Catal* 1973;28:8–19.
57. Bezerra CWB, Zhang L, Lee K, Liu H, Marques ALB, Marques EP, et al. A review of Fe-N/C and Co-N/C catalysts for the oxygen reduction reaction. *Electrochim Acta*. Submitted 2008.
58. Baranton S, Coutanceau C, Garnier E, Leger J-M. How does α -FePc catalyst dispersed onto high specific surface carbon support work toward oxygen reduction reaction (orr)? *J Electroanal Chem* 2006;590:100–10.
59. Zagal J, Sen RK, Yeager E. Oxygen reduction by Co(II) tetrasulfonatophthalocyanine irreversibly adsorbed on a stress annealed pyrolytic graphite electrode surface. *J Electroanal Chem* 1977;83:207–13.

60. Collman JP, Marrocco M, Denisevich P. Potent catalysis of the electroreduction of oxygen to water by dicobalt porphyrin dimers adsorbed on graphite electrode. *J Electroanal Chem* 1979;101:117–22.
61. Savy M, Andro P, Bernard C, Magner G. Studies of oxygen reduction on the monomeres and polymeres-i. Principles, fundamentals, and choice of the central ion. *Electrochim Acta* 1973;18:191–7.
62. Alonso-Vante N, Fieber-Erdmann M, Rossner H, Holub-Krappe E, Giorgetti Ch, Tadjeddine A, et al. The catalytic center of transition metal chalcogenides vis-à-vis the oxygen reduction reaction: an in situ electrochemical EXAFS study. *J Phys IV France* 1997;7:887–9.
63. Alonso-Vante N, Jaegermann W, Tributsch H, Honle W, Yvon K. Electrocatalysis of oxygen reduction by chalcogenides containing mixed transition metal clusters. *J Am Chem Soc* 1987;109:3251–7.
64. Alonso-Vante N, Tributsch H. Energy conversion catalysis using semiconducting transition metal cluster compounds. *Nature* 1986;323:431–2.
65. Schmidt TJ, Paulus UA, Gasteiger HA, Alonso-Vante N, Behm RJ. Oxygen reduction on $\text{Ru}_{1.92}\text{Mo}_{0.08}\text{SeO}_4$, Ru/Carbon, and Pt/Carbon in pure and methanol-containing electrolytes. *J Electrochem Soc* 2000;147:2620–4.
66. Duron S, Rivera-Noriega R, Leyva MA, Nkeng P, Poillerat G, Solorza-Feria O. Oxygen reduction on a $\text{Ru}_x\text{S}_y(\text{CO})_n$ cluster electrocatalyst in 0.5 M H_2SO_4 . *J Solid State Electrochem* 2000;4:70–4.
67. Gonzalez-Huertra RG, Chavez-Carvayar JA, Solorza-Feria O. Electrocatalysis of oxygen reduction on carbon supported Ru-based catalysts in a polymer electrolyte fuel cell. *J Power Sources* 2006;153:11–17.
68. Gochi-Ponce Y, Alonso-Nunez G, Alonso-Vante N. Synthesis and electrochemical characterization of a novel chalcogenide electrocatalyst with an enhanced tolerance to methanol in the oxygen reduction reaction. *Electrochem Commun* 2006;8:1487–91.
69. Lee K, Zhang L, Zhang J. Ternary non-noble metal chalcogenide (W-Co-Se) as electrocatalyst for oxygen reduction reaction. *Electrochem Commun* 2007;9:1704–8.
70. Pohlmann L, Tributsch H. Self-organized electron transfer. *Electrochim Acta* 1997;42:2737–48.
71. Tributsch H, Pohlmann L. Electron transfer: classical approaches and new frontiers. *Science* 1998;279:1891–5.
72. Susac D, Sode A, Zhu L, Wong P, Teo M, Bizzotto D, et al. A methodology for investigating new nonprecious metal catalysts for PEM fuel cells. *J Phys Chem B* 2006;110:10762–70.
73. Mazza F, Trassatti S. Tungsten, titanium, and tantalum carbides and titanium nitrides as electrodes in redox system. *J Electrochem Soc* 1963;110:847–9.
74. Lee K, Ishihara A, Mitsushima S, Kamiya N, Ota K. Stability and electrocatalytic activity for oxygen reduction in WC-Ta catalyst. *Electrochim Acta* 2004;49:3479–85.
75. Meng H, Shen P. Tungsten carbide nanocrystal promoted Pt/C electrocatalysts for oxygen reduction. *J Phys Chem B* 2005;109:22705–9.
76. Nie M, Shen P, Wu M, Wei Z, Meng H. A study of oxygen reduction on improved Pt-WC/C electrocatalysts. *J Power Sources* 2006;162:173–6.
77. Gordon S, Hart EJ, Matheson MS, Rabani J, Thomas JK. Reaction constants of the hydrated electron. *J Am Chem Soc* 1963;85:1375–7.
78. Sawyer DT, Sobkowiak A, Roberts Jr. JL. *Electrochemistry for chemists*. New York: Wiley, 1995; 358–402.
79. Maricle DL, Hodgson WG. Reduction of oxygen to superoxide anion in aprotic solvents. *Anal Chem* 1965;37:1562–5.
80. Peover ME, White BS. Electrolytic reduction of oxygen in aprotic solvents: the superoxide ion. *Electrochim Acta* 1966;11:1061–7.

81. Vsudevan D, Wendt H. Electroreduction of oxygen in aprotic media. *J Electroanal Chem* 1995;392:69–74.
82. Saha MS, Ohsaka T. Electrode kinetics of the $O_2/O_2^{\cdot-}$ -redox couple at Hg electrode in the presence of PVC in aprotic media. *Electrochim Acta* 2005;50:4746–51.
83. Wu J, Che Y, Okeyoshi T, Okajima T, Matsumoto F, Tokuda K, et al. Hydrodynamic chronocoulometric determination of diffusion coefficients and concentrations of dioxygen in media containing quinoline, isopuinoiline, and methyquinolines. *Anal Chem* 1999;71:4056–60.
84. AlNashef IM, Leonard ML, Kittle MC, Matthews MA, Weidner JW. Electrochemical generation of superoxide in room temperature ionic liquids. *Electrochem Solid-State Lett* 2001;4:D16–18.
85. AlNashef IM, Leonard ML, Matthews MA, Weidner JW. Superoxide electrochemistry in an ionic liquid. *Ind Eng Chem Res* 2002;41:4475–8.
86. Zhang D, Okajima T, Matsumoto F, Ohsaka T. Electrochemical reduction of dioxygen in 1-n-alkyl-3-methylimidazolium tetrafluoroborate room temperature ionic liquids. *J Electrochem Soc* 2004;151:D31–7.
87. Katayama Y, Onodera H, Yamagata M, Miura T. Electrochemical reduction of oxygen in some hydrophobic room temperature molten salt systems. *J Electrochem Soc* 2004;151:A59–63.
88. Yang H, McCreery RL. Elucidation of the mechanism of dioxygen reduction on metal free carbon electrodes. *J Electrochem Soc* 2000;147:3420–8.
89. Choi Y, Chjo K, Park S. Oxygen reduction at Co(II)2-disalophen modified carbon electrodes. *J Electrochem Soc* 1995;142:4107–12.
90. Song C, Zhang L, Zhang J. Reversible one-electron electro-reduction of O_2 to produce a stable superoxide catalyzed by adsorbed Co(II) hexadecafluoro-phthalocyanine in aqueous alkaline solution. *J Electroanal Chem* 2006;587:293–8.
91. Chevalet J, Rouelle F. Electrogenation and some properties of the superoxide ion in aqueous solutions. *J Electroanal Chem Interf Electrochem* 1972;39:201–16.
92. Beyer W, von Sturm F. Polarographic reduction of oxygen in presence of phthalocyanine complex. *Angew Chem* 1972;84:154–5.

PEM Fuel Cell Electrocatalysts and Catalyst Layers
Fundamentals and Applications

Zhang, J. (Ed.)

2008, XXI, 1137 p., Hardcover

ISBN: 978-1-84800-935-6